LUIS CARLOS COLOCHO HURTARTE

PLANT NITROGEN STATUS DRIVING SOIL ORGANIC MATTER MINERALIZATION IN THE RHIZOSPHERE

Dissertação apresentada à Universidade Federal de Viçosa, como parte das exigências do Programa de Pós-Graduação em Solos e Nutrição de Plantas, para obtenção do título de *Magister Scientiae*.

VIÇOSA
MINAS GERAIS – BRASIL
2017

Ficha catalográfica preparada pela Biblioteca Central da Universidade Federal de Viçosa - Câmpus Viçosa

T
C718p
2017

Colocho Hurtarte, Luis Carlos, 1989-
Plant Nitrogen status driving soil organic matter mineralization in the rhizosphere / Luis Carlos Colocho Hurtarte. – Viçosa, MG, 2017.
ix, 51f. : il. (algumas color.) ; 29 cm.

Inclui anexo.
Orientador: Ivo Ribeiro da Silva.
Dissertação (mestrado) - Universidade Federal de Viçosa.
Inclui bibliografia.

1. Plantas e solo. 2. Solos florestais. 3. Solos - Teor de compostos orgânicos. 4. Solos - Humus. 5. *Eucalyptus ssp*.. 6. Plantas - Metabolismo. I. Universidade Federal de Viçosa. Departamento de Solos. Programa de Pós-graduação em Solos e Nutrição de Plantas. II. Título.

CDD 22 ed. 631.43

LUIS CARLOS COLOCHO HURTARTE

PLANT NITROGEN STATUS DRIVING SOIL ORGANIC MATTER MINERALIZATION IN THE RHIZOSPHERE

Dissertação apresentada à Universidade Federal de Viçosa, como parte das exigências do Programa de Pós-Graduação em Solos e Nutrição de Plantas, para obtenção do título de *Magister Scientiae*.

APROVADA: 26 de janeiro de 2016.

Samuel Vasconcelos Valadares

Rogério Faria Vieira

Leonardus Vergütz
(Coorientador)

Ivo Ribeiro da Silva
(Orientador)

AGRADECIMENTOS

À Universidade Federal de Viçosa e ao Departamento de Solos, por possibilitar a realização deste curso de mestrado.

À CAPES, FAPEMIG, CNPq, SIF e ao Grupo NUTREE pelo auxílio financeiro

Aos Professores Ivo Ribeiro da Silva e Leonardus Vergutz, pelos ensinamentos, discussões e confiança acompanhados de momentos de descontração nestes anos.

Ao Prof. Mauricio Fontes e a Rogerio Faria pelo incentivo e ajuda no início da graduação.

Aos demais Professores do Departamento de Solos, por contribuírem para minha formação, em especial Victor Hugo, Jaime Mello, Júlio César Lima Neves, Nairam Félix de Barros e Maurício Fontes.

Aos funcionários do DPS e da Pós-graduação.

Aos técnicos do Laboratório de Isótopos Estáveis (LIE) João Milagres e Humberto, pela constante ajuda, paciência e pela importante contribuição para a realização deste trabalho.

Aos estagiários pelas contribuições na execução dos experimentos, em especial a Gabi e Crock (Rodrigo).

Aos colegas da Pós-graduação e do LIE, em especial Ricardo, Fernanda Caparelli, Daniela, Marina, Ana, Helen, Gabriel (Tcha), Medina, Ivan, Luis Bola, Gustavo, Chico Bento, Matheus Barreto, Rafael, Crock e Luiz.

Aos membros da banca Rogerio, Samuel e Leonardus pelas sugestões que levaram à melhoria da qualidade do trabalho.

Aos amigos do intercambio em especial Bruno, Daniel, Marco, Lobão, Fábio, Maria, Thera e Alexandre.

A meus queridos pais, Jose Luis Colocho e Maria Margarita e minha irmá Ana Elena pelo constante apoio e incentivo, são vocês que fazem tudo valer a pena.

Aos meus amigos/irmãos de Viçosa Rodrigo, Álefe, Conrado e Josimar, agradeço pela força nos momentos difíceis e pelas risadas no dia a dia.

BIOGRAFIA

LUIS CARLOS COLOCHO HURTARTE, filho de Jose Luís Colocho Ortega e Maria Margarita Hurtarte, nasceu no dia 06 de dezembro de 1989, em Viçosa/Guatemala – MG.

Em dezembro de 2007 concluiu o ensino médio no English American School em Guatemala e em agosto de 2009 foi aprovado em primeiro lugar por transferência para a Universidade Federal de Viçosa no curso de Agronomia, concluindo em janeiro de 2015.

Entre agosto de 2012 e marco de 2014 foi bolsista do programa Ciência sem Fronteiras/CNPq na modalidade "graduação sanduiche", na Universidade Técnica de Munique (Technische Universitaet Muenchen), sob orientação dos Professores Thilo Rennert e Joerg Prietzel.

Em marco de 2015, ingressou no Programa de Pós-graduação em Solos e Nutrição de Plantas da Universidade Federal de Viçosa, em nível de Mestrado sob orientação do Professor Ivo Ribero da Silva.

A mediados de 2016 foi aprovado nos programas de doutorado completo tanto Instituto Max Plack de Biogeoquimica pela International Max Planck Reseach School on Global Biogeochemical Cycles e na Universidade Técnica de Munique.

Em janeiro de 2017 submete-se a a defesa de com a dissertação titulada: "Plant Nitrogen status driving soil organic matter mineralization in the rhizosphere".

SUMÁRIO

RESUMO

HURTARTE, Luis Carlos Colocho, M.Sc., Universidade Federal de Viçosa, janeiro de 2016. **Plant Nitrogen status driving soil organic matter mineralization in the rhizosphere.** Orientador: Ivo Ribeiro da Silva. Coorientadores: Leonardus Vergutz e Mauricio Dutra Costa

Os fatores que regulam a dinâmica do Carbono (C) e Nitrogênio (N) do solo na rizosfera são ainda pouco compreendidos. A mineralização de C na rizosfera pode ser fortemente influenciada pelo estado nutricional da planta, a concentração de CO_2 na atmosfera e a temperatura do ambiente, entre outros. Em este estudo, avaliamos o status nutricional de N em plantas de *Eucalyptus spp.* e sua influência na dinâmica do C e do N na rizosfera. Realizamos um experimento usando um rhizobox dividido em dois compartimentos. No compartimento de cima plantas foram cultivadas em areia lavada e supridas com uma solução nutritiva contendo todos os nutrientes e a mesma solução porem sem N. No compartimento inferior o contato das raízes com o solo foi limitado usando uma membrana de nylon com abertura de 5 µm. Observamos uma maior razão raiz:parte aérea e maiores concentrações de CO_2 no solo das plantas com deficiência de N. As raízes das plantas deficientes em N, apresentaram maiores concentrações em relação as plantas não deficientes em N, de citrato e tallose, e menores concentrações de sucrose e aminoácidos. A análise de C e N da fração de matéria orgânica ligada aos minerais, junto com os dados obtidos pela termoquimolise indicam um aumento na mineralização de C e uma modificação na dinâmica do N. Devido a impossibilidade de contato físico direto com o solo, pela presença da membrana de nylon, a única forma de modificar o solo seria então pela exsudação de compostos pelas raízes. O contrastante conteúdo de aminoácidos e açúcares na raiz, junto com os dados do extrato da solução do solo e de mineralização de C, indica que a composição destes exsudatos diferiu em razão da deficiência de N. Enquanto as plantas deficientes em N exsudaram mais ácidos orgânicos, as plantas com ótimo status nutricional foram capazes de exsudar compostos energeticamente ricos. Os dados de $\delta^{13}C$ da matéria orgânica ligada aos

minerais indica que as plantas deficientes em N afetaram um maior volume de solo que as plantas supridas de N. Tudo isto mostra que, diferentes mecanismos de efeito priming foram dominantes, dependendo do status nutricional da planta. Em plantas deficiente de N, a mineralização de C no solo foi dominada pelo mecanismo chamado de “mineração de N”, enquanto no solo das plantas supridas de N o mecanismo dominante foi a “estequiometria microbiana”. Este trabalho demostra pela primeira vez, ao nosso saber, a atuação de diferentes mecanismos de efeito priming na mesma planta, sobre diferente status de N. Assim ressaltando, a importância do manejo de nutrientes na dinâmica do C da rizosfera.

ABSTRACT

HURTARTE, Luis Carlos Colocho, M.Sc., Universidade Federal de Viçosa, January, 2016. **Plant Nitrogen status driving soil organic matter mineralization in the rhizosphere.** Adviser: Ivo Ribeiro da Silva. Co-advisers: Leonardus Vergutz and Mauricio Dutra Costa

The factors that regulate the dynamics of soil Carbon (C) and Nitrogen (N) in the rhizosphere are still poorly understood. The soil C mineralization in the rhizosphere can be heavily influenced by plant's nutritional status, atmospheric CO_2 concentration and temperature, among others. In this study, we assess the influence of *Eucalyptus spp*. N status on the C and N dynamics in the rhizosphere. We performed an experiment using two compartment rhizobox. In the upper compartment, plants were cultivated in washed sand and supplied with a solution containing all nutrients or all nutrients but N. The lower compartment limited the contact of the roots with the soil using a 5 µm mesh nylon membrane. We observed a higher root-shoot ratio for the N deficient plants and an increase in its soil CO_2 concentration. The roots of the –N planted treatment had higher concentrations of citrate and tallose and lower concentration of sucrose and aminoacids, when compared to the +N planted treatment. The C and N analysis of the mineral associated organic matter fraction, together with the thermochemolysis data showed an increase in C mineralization in both planted treatments and changes in N dynamics. As the roots had no physical contact with the soil due to the nylon membrane, the changes in the soil must have been consequence of root exudation. The contrasting sugar and aminoacid root content, together with the citrate concentration in soil solution extract and the C mineralization data, indicate that exudate composition changed due to the plants N status. The data indicates that the plants in the –N treatment exudated more organic acids than the plants of the +N treatment. Still the exudate composition of the plants with the +N treatment may had a higher energetic content and thus affected differently the soil microbial communities. The $\delta^{13}C$ data indicate that the N deficient plants affected a higher volume of soil than the plants of the +N treatment. All this together shows different priming mechanisms were

dominant due to the plants N status. As the plants were N deficient, the mineralization of soil C was driven by the “N-mining” mechanism while in the soil of the +N planted treatment the dominant mechanism was “microbial stoichiometry”. This work demonstrates, to our knowledge, by the first time using the same plants, different priming mechanisms due to the plants N status. Thus highlighting, the importance of plants nutrient management in the rhizosphere C dynamics.

INTRODUCTION

The global terrestrial carbon (C) balance is mainly driven by forests (Jobbágy and Jackson, 2000), which together cover ~30% of the boreal, temperate and tropical land surface (Bonan, 2008). The C balance can be affected by the ecosystem's health (Trumbore et al., 2015) (eg. nutrient deficiency, CO_2 fertilization, diseases, etc), which in turn is affected also by climate change. This occurs because climate influences several important variables for the ecosystems health such as temperature, CO_2 and N balance. As it has recently been exposed (He et al., 2016) soils might not be an effective C sink as it was previously thought. However soils still hold a major role as a source of various greenhouse gases (Amundson et al., 2015). Therefore, it is important to assess and correctly model the responses of forests to climate change and how this feedback will affect the terrestrial carbon balance (Bonan, 2008; Heimann and Reichstein, 2008; Trumbore et al., 2015).

Forests contribute to the net C balance by either acting as a source or a sink of CO_2. When acting as a sink, a large part of the forest C can be stored in the soil. The main input of C to the soil are the roots together with microbial derived compounds (Jones et al., 2009; Kallenbach et al., 2016; Rasse et al., 2005) especially in the subsoil (Rumpel and Kögel-Knabner, 2011).

The transfer C to the soil can increase or inhibit soil organic matter (SOM) mineralization. This phenomena is known as rhizosphere priming

(Kuzyakov, 2002). The roots can promote the priming effect by exudating different organic compounds (Paterson et al., 2007). The roots change its exudate composition as a physiological response of the plants to abiotic and biotic stresses, for instance nutrient limitations (Dijkstra et al., 2013; Kuzyakov, 2002; Wieder et al., 2015).

In a changing climate panorama, the nutrient requirements of forest may shift and when deficient, plants may scavenge for nutrients by mineralizing the SOM (Heimann and Reichstein, 2008). This is especially true for N, which is a limiting nutrient in several ecosystems. An increasing concern on the N-climate feedbacks has drawn interest in coupling the effects of N deficiency to climate variables, such as CO2 increase (Hungate, 2003). Still up to this day, few experiments are able to confidently, separate the effects of N deficiency in the plants exudates, and its effect on SOM mineralization. Only a hand full of experiments most of them using artificial exudates have tackled this problem (Drake et al., 2013; Meier et al., 2017).

In the tropics the Eucalypt forests are within one of the most productive ecosystems in the globe (Stape et al., 2004). Although much is known about the tree, a conundrum has emerged regarding the lack of response to N fertilization and its high N requirements. The current most accepted hypothesis is that the trees promote SOM to access more N. This may be true as Eucalyptus' roots exudate large amounts of organic acids, which increase under abiotic stresses such as high Al concentrations (Silva et al., 2004).

Here we attempt to take a step further in the N climate feedbacks by unraveling the rhizospheric N-driven priming processes, through a rhizobox experiment. The main objective of this study was to assess the possible mechanisms for rhizospheric priming effect in a representative tropical soil cultivated with *Eucalyptus spp*. We aimed to achieve this by, assessing (i) the effects of N fertilization in the root's traits and physiology. (ii) Reviewing the changes in soils properties such as mineralogy, pH, C and N content and organic acids in its soil solution, and finally by (iii) relating the plants N-status to changes in the molecular composition of SOM in the rhizosphere.

MATERIALS AND METHODS

Experimental set-up

The experiment was conducted using a rhizobox system designed by Wenzel et al., (2001). This system is composed of two physically separate compartments: an upper compartment containing washed < 2 mm sand in which the plants were cultivated and a lower compartment containing soil. The upper compartment has a narrow slit in its bottom, through which plant roots can vertically penetrate in the lower compartment. The contact of the roots with the soil in the lower compartment is limited by a nylon membrane with a pore size of 5 µm (Tegape). See schematic representation of the rhizobox in the Supplemental Figure 1.

The rhizobox system made possible to modify the nutritional status of the plants without modifying the nutrient content of the soil. This was done by applying to the upper compartment different nutrient solutions, conducted by glass fiber wicks (Fiberseals). We performed a factorial experiment with two factors with two levels each.

The first factor was the plant effect, thus rhizoboxes were assembled with plants (+Pl) or without plants (-Pl). The plants used for the experiment were commercially available 3 months old *Eucalpyptus grandis x Eucalyptus urophylla* clonal seedlings. The second factor was the N effect, a complete modified Clark solution (+N, with a labeled ^{15}N - 2% APE) or an incomplete one (-N) was supplied to the upper compartment, details of the Clark solutions are in the Supplementary Table 1. Three repetitions of each treatment were assembled, a scheme of the experiment can be found in the Supplementary Figure 2.

The lower compartment was filled with soil collected from a cultivated tropical pasture (*Brachiaria decumbens* - 20 years) in Paula Candido, Minas Gerais – Brazil (20° 52' S, 42° 58'E). This pasture field (*Brachiaria decumbens)* is a C-C4 species and its cultivation after a C-C3 native forest lead to an increase in the soil $^{13}C\delta$ from -27 to -16.75 ‰, thus allowing us to track the root derived C in the soil. The soil was classified as a Ferrasol (Typic Hapludox according to the U.S. Soil Taxonomy) loamy texture, pH_{H2O} of 5.24, total organic carbon of 25.4 g/kg of C (± 0,92).

A soil-air probe was placed in the lower compartment, which consisted of a silicone rubber tube. The tube was 20 cm long, with a 5 mm internal diameter and a 1 mm width. It was accommodated spirally in the center of the box. The silicon tube was connected to a 15 cm copper tube, that crossed through and projected out of the upper box. The copper tube's ending was kept shut using a three way stopcock (Supplementary Figure 2 - Kammann et al., 2001).

The experiment took place in a growth chamber (temperature of ~25 °C and air relative humidity of ~ 60%). Plants were grown in the upper compartment, and after 20 days the complete rhizobox was assembled. The rhizoboxes were kept each inside a 30 L polyetilene black box in order to avoid light disturbance to the roots. Plants were cultivated for 30 days after the roots started to penetrate in the lower compartment.

The day before unmounting the experiment, rhizoboxes were covered using an acrylic chamber and pulse-labeled with ^{13}C (Machado et al., 2011). The following day, the SPAD index of the plant middle leaves was measured using a Chlorophyll meter SPAD-502Plus (Konica Minolta – Japan).

The soil air samples were taken using a 5 ml syringe, transferred to previously evacuated 12 ml exeteiners. The samples were analyzed for C-CO_2 and $^{13}C/^{12}C$ of C-CO_2 relative to the PDB internal standard in an *Isotopic Ratio Mass Spectrometer- IRMS* (ANCA-GSL, 20-20, Sercon, Crewe, UK). Then, the plants were taken out of the polyethylene boxes and the formed root mat in the lower

compartment was photographed, collected and immediately freezed in N_2 and kept in an ultrafreezer at -80 °C until further analysis.

The above ground material was also collected, separated in grown before (old) and after (new) the experiment started. The samples were dried in a forced air furnace, weighted, milled and kept in airtight boxes until further analysis.

Finally, the rhizoboxes were opened and the soil moisture was probed using a sensor (EC-5, Decagon, Pullman, WA). The soil was sectioned in three distances parallel to the root mat (0 - 3 mm, 3- 6 mm and 6 -15 mm) using a modified microtome from Fitz et al., (2003). The samples were divided in two, one subsample was used to extract the soil solution according to Pérez et al. (2002). The remaining soil sample and the soil solution were kept in an ultrafreezer until further analysis.

Bulk analyses

The soil samples were freeze-dried and divided in two, these were used to (i) measure the pH in water according to (Pansu and Gautheyrou, 2006) and (ii) to physically fractionate the SOM according to Cambardella and Elliott (1992). The fractions were designated as particulate organic matter (POM >53 µm) and mineral associated organic matter (MAOM < 53 µm). The fractionation was performed by dispersing 3 g of the sample in sodium hexametaphosphate, and sieved at 53 µm. The two fractions were dried in a forced air oven at 50 °C, and kept in airtight boxes until further analysis.

The OC, N content and $^{13}C/^{12}C$ and $^{15}N/^{14}N$ ratios of the MAOM fraction was determined. The changes in short-range-order and organic bound Fe and Al oxyhydroxides were assessed by independent oxalate and pyrophosphate extraction and analyzed by atomic absorption spectrometry (Shang and Zelazny, 2008).

Rhizospheric soil solution analysis

The extracted soil solution was freeze dried and reconstituted in 1 ml of ultra-pure water and passed through a 0.45 µm membrane. An aliquot of 0.5 ml was diluted in 2 ml of ultrapure water and analyzed for organic acids by ion exchange chromatography (Silva et al., 2004).

Root image analysis and metabolic profiling

The photographed roots were analyzed using the GiaRoots software (Galkovskyi et al., 2012), the cropping tool was used to select the root mat area and the scale was manually defined. The root identification parameters were chosen for each photo individually using the double adaptive image thresholding. The computed traits were: average root width, root area, length, surface area and specific root length.

The extraction and identification of compounds produced by the roots in the lower box, with possible involvement in the rhizospheric priming effect was made following the method from (Lisec et al., 2006). Briefly, root tissue (100 mg) were homogenized with liquid nitrogen and extracted in 1.4 mL of methanol, and 60 µL of internal standard (0.2 mg ribitol/mL water) was

subsequently added as a quantification standard. The mixture was extracted for 15 min at 70 °C and mixed vigorously with 1.4 mL of water. In order to separate polar and nonpolar metabolites, 750 µL of chloroform was added to the mixtures. After centrifugation at 2,200 *g*, the upper methanol/water phase was taken ad reduced to dryness in vacuum. The sample was resuspended and derivatized in 40 µL of 20 mg/mL methoxyamine hydrochloride in pyridine at 37 °C for 120 min. Afterwards, the extract was treated with 60 µL of N-methyl-N-[thrimethylsilyl]trifluoroacetamide at 37°C for 30 min. A standard alkane mixture (n-dodecane, n-pentadecane, n-nonadecane, n-docosane, n-octacose, n-dotracontane and n-hexatriacontane) dissolved in anhydrous pyridine (0.029% [v/v]) was added before trimethylsylation for retention time control. Sample volumes of 1 µL were analyzed in an Shimadzu QP 2010-SE GC/MS, equipped with a Rtx-5MS capillary column (Restek, Bellefonte, CA – USA). The chromatograms and mass spectra were evaluated using the GCMSolution software. Compounds were indenfied by their mass spectra and retention time index matching to the mass spectral collection of the NIST11 database. Numerical analyses were based on the peak height values of the recorded mass feature. These values were corrected for the dry weight of each sample and by the response of the internal standard from each respective GC-MS chromatogram to obtain normalized responses.

MAOM molecular characterization using TMAH-GC-MS

The changes in the molecular organic compounds of the MAOM fraction were assessed using off-line tetramethyl ammonium hydroxide

(TMAH) mediated thermochemolysis (del Rio et al., 1998). The TMAH-thermochemolysis, products were analyzed by gas chromatography-mass spectrometry in a Shimadzu QP 2010-SE GC-MS equipped with a Rtx – 5MS column (30 m length; 0.25 mm ID; 0.25 µm film thickness). Ultrapure He was used as the carrier gas at a flow rate of 3 mL min^{-1}, the ion source temperature set to 200 °C, the interface temperature to 290 °C and oven temperature ramp from 60 °C to 300 °C at a rate of 15 °C min^{-1}. The eluted compounds in the chromatograms were identified using the NIST 2011 mass spectral library and external standards.

Synchrotron XRD analysis coupled to EGA-MS

In order to assess possible changes in the soil mineralogy and thermal resistence of the SOM to degradation, synchrotron XRD analysis coupled to Evolved Gas Analysis through mass spectrometry (EGA-MS) was performed in the Brazilian Synchrotron Light Source. Briefly, 100 mg of the MAOM fraction of each treatment and from the 0-3 and 3-6 mm distances were heated while XRD analysis was performed. This was acomplished by coupling an "Anton Paar XRK900" furnace to the beam end station and heating the sample from room temperature up to 500 °C, under an air flow of 150 mL/min (80% He, 20% O_2) at a heating rate of 5° C/min. The evolved gases were sampled and analyzed throughout the course of the whole heating process by a coupled mass spectrometer (QMA 200 - Pfeiffer Vacum). The monitored m/z values were 17 and 18 (OH and H_2O), 27 (HCN), 28 (CO), 30 (NO), 44 (CO_2 and

N_2O) and 46 (NO_2).The XRD patterns were constantly taken between 10 and 50 2θ degrees through the whole time the thermal analysis was carried out.

The EGA-MS data for H_2O and CO_2 were analyzed using the software Peakfit by adjusting exponentially modified Gaussian functions for signal deconvolution and area calculation. The XRD patterns were analyzed using the XPowder software for peak identification, peaks FWMH (full width at peak half maximum) of selected clay minerals and phase change through the heating process.

Statistical analysis

The assumptions for homogeneity of variances and normality were tested for each sample by Levene's test and Kolmogoroff-Smirnoff test respectively. Differences in the above ground material, the root dry mass, root traits and CO_2 concentrations were tested using confidence intervals ($p < 0.05$). Changes in the soils physico-chemical characteristics were tested using a two-way ANOVA followed by Dunnett-test ($p < 0.05$). All analyses were performed in the STATISTICA software (Statsoft Inc.).

RESULTS

Shoot and root changes due to N-deficiency

The N deficiency in the aboveground material heavily affected the assessed characteristics (Table 1). The new aboveground mass in the +N treatment was higher than that in the –N treatment. When analyzed the leaves

through the SPAD index, a higher N leaf content in the +N treatments against that of the –N treatment was observed.

The root mass grown in the lower compartment box was equal for both N treatments. Still the Root:Shoot ratio was significantly higher for the plants of the –N treatment than for the +N treatment. The main root trait assessed through the GIAroots software was the surface area, which was higher in the –N treatment than in the +N treatment (Table 2). This was expected as the roots of the -N treatment were highly branched and developed to second and third order. The roots from the +N treatment instead were less branched and thicker (Supplementary Figure 4). As expected, more branched roots led to higher surface area than less branched roots.

A preliminary evaluation of the metabolic profiling showed higher and equal concentrations of citric acid and oxalic acid respectively, in the root tissue of the N-unfertilized treatment (Fig. 1). Among the sugars examined lower concentrations of sucrose and fructose were observed in the roots of the N-unfertilized plants. Still higher concentrations of tallose were found in the in the roots of the N-unfertilized plants. Several aminoacids were examined, and in all cases the roots of the N-fertilized plants showed higher concentrations.

The concentration of CO_2 in the soil within the no plant controls (+N & -N) and the +N planted treatment were similar. However, the –N planted treatment attained significantly higher CO_2 concentrations (Fig. 2).

Changes in Soil properties

The unplanted +N treatment presented no differences from the unplanted -N treatment, signifying that no changes within the lower compartment are due direct N addition (Fig. 3). The MAOM fraction suffered changes from the cultivation with Eucalyptus both +N and -N. The C content of the MAOM fraction decreased for both planted (-N and +N) treatments within the first 3 mm when compared to the no plant controls. This decrease only continued for the planted –N treatment up to 6 mm from the root plane.

An increase of the MAOM $\delta^{13}C$ of both planted treatments (+N and -N) in comparison to the control was observed. The extracted soil solution presented a similar had higher concentrations of citrate in both planted treatments than in the unplanted controls. This difference between the planted treatments and the control decreased along the axis. The changes in the MAOM total N content were very contrasting for the planted treatments within the first 3 mm, increasing to 5 % for –N planted treatment and decreasing by 7 % in the +N planted one.

Changes in extractable Fe and Al from the MAOM fraction were assessed through the oxalate-citrate method. These decreased for Fe and only in the distance up to 3 mm for the –N planted treatment, relative to the no plant control. No significant change was observed in oxalate extractable Al, for both planted treatments (+N and –N) relative to both controls (+N and –N).

Changes in pH in both planted treatments of up to 0.6 pH units less than that of the unplanted control were observed. This values were maintained within the whole 15 mm of the –N planted treatment. The +N planted treatment, however, had a soil pH decrease only within the first 3 mm.

Synchrotron XRD and EGA-MS

Kaolinite, gibbsite and goethite were the main clay minerals found in the MAOM fraction of the soil we used. The main features of Kaolinite, Gibbsite and Goethite were investigated through synchrotron XRD at room temperature, and are summarized in the Table 3. No changes were seen in neither the d spacing or FWMH of Kaolinite or Gibbsite's main peaks in any treatment. However, changes in d spacing and FWMH are observed in the Goethite peak of the –N planted treatment, going from 0.826 for the controls to 0.531. The d-spacing of goethite's 101 hkl in the same treatment, had also an slight change going from 4.15 to 4.13.

Changes in CO_2 evolution from the thermal decomposition of the MAOM fraction, within the temperatures ranges of 155, 320 and 500 °C are summarized in Table 3. At the first 3 mm, the MAOM fraction from both planted treatments (+N and –N) had a similar decrease of CO_2 evolution compared to the unplanted controls. Nevertheless, the MAOM of the planted –N treatment had a much stronger decrease of CO_2 evolution in the temperature ranging of up to 500°C, within the same 3 mm. At the second distance (3 – 6 mm), the +N planted treatment increased its CO_2 evolution by

up to 14 % within the first 155 °C, and decreased it by 9% within the 320° C range, in relation to the –N unplanted control.

The CO_2 evolution pattern from the MAOM fraction of the –N planted treatment within the second distance had a similar behavior to that of the first distance (0 – 3). Nevertheless, the decrease in CO_2 evolution from the first 155 ° C was less pronounced than that in the first 3 mm. No significant change was observed in the CO_2 evolution within the 500 °C range for both planted treatments at the second distance.

Molecular characterization of organic compounds in the MAOM fraction

At the termination of the study, we performed an off-line TMAH-GC/MS to examine the molecular composition of organic compounds in the MAOM fraction separately from soils collected at different distances from the root plane (Fig 4). The molecular characterization of the compounds in the unplanted treatments provided controls to compare changes in SOM chemistry following the rhizosphere priming. A detailed table of all identified compounds in each treatment at each distance can be viewed in the supplementary material (Supp. Tables 4, 5 and 6). At the no plant controls, a rather high abundance of aliphatic compounds was observed, together with suberin derived and N-bearing compounds. These relative abundances were consistent along the whole axis. The aliphatic compounds were always the dominant group in all samples. At the closest distance, an accumulation of N-bearing compounds and a decrease of aliphatic compounds was observed in the MAOM fraction of the –N planted treatment and the opposite effect

(decrease of N-bearing and increase of aliphatic compounds) in the same fraction of the +N planted treatment.

At the second distance, the proportional difference between the controls and the –N planted treatment treatment started to fade away. Still a higher number of aliphatic compounds were identified for the –N planted treatment and a higher proportion of N-bearing compounds were found in the +N planted treatment. Along the whole axis in all samples no relative abundance differences for the cutin and suberin derived compounds was observed.

DISCUSSION

Effects of N fertilization on root morphology and physiology

We evaluated the effect of *Eucalyptus spp.* rhizodeposition on mineral bound SOM by employing the rhizobox system developed by Wenzel et al., (2001). This system allowed us to both cultivate plants under optimal N and other nutrients supply and without N supply via the upper compartment, having the advantage of no direct interference from nutrient addition with the rhizospheric soil in the lower compartment. It also enabled us to assess the effects of only rhizodeposition, without the physical effects of roots on soil (eg. disruption of aggregates, C and N contribution of dead roots, etc). The membrane's mesh (5 µm) guaranteed that no root hair came in direct contact with the soil, thus safekeeping that the effects of the planted treatments on the soil are only result of plant rhizodeposition.

The nitrogen status affects plants in a great manner, as N is required to synthetize amino acids, nucleotides and secondary metabolites that have direct roles in plant signaling, structure and adaptation (Tschoep et al., 2009). Thus, it was no surprise that, in the current experiment a greater shoot dry mass was produced by +N planted treatments. Physiological changes in the plant due the lack of N led to smaller and yellow leaves in the –N planted treatments. This response is directly related to the lack of N, as it is necessary for chlorophyll synthesis, leading to lower CO_2 fixation and thus less C for structural and physiological functions (Hermans et al., 2006). This imbalance led to important changes in the source/drain functions of C and N in the plant, as it can be observed by the metabolic profiling data (Fig 1)

The rhizobox design allowed us to efficiently assess root morphology and characteristics. This because the removal of the roots in the lower compartment was quick and without causing notable damage. Our results show that when lacking N, plants invested C to develop thinner and longer roots (Table 2). These thinner roots will in turn exudate more and have a larger surface area (Ostonen et al., 2007) optimizing nutrient uptake and increasing its effect on the adjacent soil. Our results are line with the observations shown by Marschner et al., (1996) and by Hermans et al., (2006), who showed that under N deficiency plant partition of photoassimilates changed, redirecting more C to its roots.

Our root metabolic profile of the –N planted treatment, showed no accumulation of sucrose in the root tissue, but of other sugars like tallose.

This in turn may have regulated gene expression leading to more cell division and elongation (Koch, 2004). No accumulation of amino acids in the –N planted treatments was observed, when compared to the +N planted treatment. We hypothesize that it was possibly to a preferential accumulation in the leaves.

Our results of root dry mass in the lower box are in line with those by Jourdan et al., (2008), who in a field experiment showed that in the absence of N, *Eucalyptus spp.* produces a greater root mass than when fertilized with N. Even though our root dry mass was the same for both treatments the root:shoot ratio increased under N deficiency, this concurs with the barley data from Farrar et al., (2003), thus implying a higher C investment in root formation.

Rhizospheric priming as function of plant N status

The plants distinct N status resulted in different effects on the rhizospheric soil. A first sign of the plant-induced changes in both N-fertilized and unfertilized rhizosphere soils is the different soil air CO_2 concentrations. The contrasting CO_2 values, higher in the unfertilized treatment might be result of either higher respiration by the roots of the unfertilized treatment, due to a higher C translocation to the root and higher activity (Marschner et al., 1996). More likely, however, the greater soil air CO_2 is the result of a plant-root induced SOM decomposition by the higher heterotrophic microbial activity (Kuzyakov and Blagodatskaya, 2015).

As we further analyzed different physico-chemical parameters in the soils it became apparent that different mechanism for priming were in action depending on the N status of the plants (Fig. 3). A higher C mineralization in both treatments (Fig. 3 a) indicates that even at optimal N status *Eucalyptus spp* may induce a priming effect at the closest distances to the root. We believe that this priming was caused by the optimal exudate composition in the N-fertilized treatment. Since there was no imbalance of sugars, aminoacids and organic acids in the N-fertilized roots, the same may be true for its exudate. Thus, the increased C mineralization may be due to microbial stoichiometric constraints. This, is in line with the work of Drake et al., (2013), were C-N balanced artificial exudate solution induced a positive priming by providing N rich substrate for the microorganism to synthetize exoenzymes

Although the changes in C within the first distance do not differ for both treatments, in the second distance (3 – 6 mm) a higher mineralization in the unfertilized treatment was observed, similar behavior presented the pH and Feox. As higher citrate concentrations were found in the N-unfertilized roots and MAOM fraction (Fig 3. c), we believe that the unfertilized *Eucalyptus* exudated compounds with more of a complexing behavior in order to have access to the N in the mineral bound organic matter. As reviewed by Furrer and Stumm, (1986) and Zinder et al., (1986), citrate and oxalate are important Fe and Al complexants with high dissolution rates. The activity of such organic complexants in the unfertilized treatment was confirmed by a

decrease in Feox(Fig 2 d), and by shifts in the d-spacing and FWHM of goethite (Table 3 and 4), while at the fertilized treatment no significant changes were observed.

The N content at the MAOM fraction of both planted treatments had contrasting values (Fig.3 b), as the –N planted treatment increased and the +N planted treatment decreased. This led us to believe that a different microbial dynamic acted as a driver for either the accumulation or the depletion of N near the roots. Plants change its exudate composition due to nutrient status (Carvalhais et al., 2011), and that way benefit/affect different microbial communities. As Dijkstra et al., (2013) expressed, as a easily metabolizable C is made available for microorganisms, opportunistic communities (r-strategist) may rose to higher populations than that of the native slow growth communities (K-strategist).

The plants under N deficiency tried to supply themselves with N through other mechanisms like higher root branching and higher organic acid exudation. Due its N deficiency, we believe that sugars and N-bearing compounds were instead accumulated in the leaves as it has already been observed in other plants under N deficiency (Paul and Driscoll, 1997) and this can act as signal for root elongation and growth (Hermans et al., 2006). Together with the organic acid exudation, a rather high change in soil pH was observed (Fig.2 f), which may have been the consequence of the high CO_2 concentration or due the plant proton extrusion. Either way, these changes

may have furthered the dissolution of Fe oxy(hydro)xides by lowering the Eh and pH of the solution.

The unfertilized plants priming mechanism made mineral bound SOM available for the microbial communities. The higher C availability lead to a microbial population increase, specifically the r-strategists as these are the ones better prepared for native OM mineralization (Philippot et al., 2013).

Differences in the mineralized C and N at the vicinity of the roots was also confirmed by EGA and TMAH- GC/MS (Table 3 and Fig. 4). The EGA-MS CO_2 evolution showed rather high C differences between the MAOM fraction from the fertilized and the unfertilized treatments within the C fraction thermally resistant fraction (between 300 and 500 °C). The CO_2 derived from the MAOM fraction continued to differ at the second distance, except that there were also lower areas within the more thermally labile C fractions (155 – 300 °C). We believe that this differences are due changes in the chemical composition of the mineral bound SOM fraction.

The TMAH-GC/MS data confirmed what the bulk analysis showed for the unfertilized treatment, an increase of N-bearing compounds in the vicinity of the root plane and a decrease in aliphatic compounds, which could explain the main changes in the pattern of CO_2 evolution from thermally decomposition of the MAOM fraction of SOM. Although in both planted treatments (+N and –N) the C decrease was the same, the molecular constitution of each was different, as the MAOM fraction from the fertilized

and planted treatment had a much higher content of aliphatic compounds than even the no plant controls.

We believe that such contrasting effects in SOM chemistry among the treatments was due to a differential response of the dominant microbial communities and caused by the variable composition of exudates. Although root exudation is independent of the N-status, the chemical composition of the exudates is bounded to the plant N status. Thus, the microbial communities benefited are consequence of the plants nutritional necessities.

Implications for C dynamics

In this experiment, we had anticipated that the soil under N-unfertilized plants would give a higher SOM mineralization due to a positive priming effect. Although this was true, we did not expect to have also a positive priming effect in the N-fertilized treatment. This led us to believe that even though in both N treatments the plants induced SOM mineralization, different mechanisms of priming were under effect, which affected the SOM chemistry in different ways.

While both planted treatments increased C mineralization, the N-deficient plants affected a higher rhizospheric soil volume. This larger effect was due a combination of changes in physicochemical factors (soil pH, CO_2 concentration) and a higher exudation of organic acids.

The Figure 5 (modified from (Chen et al., 2014)) illustrates the dominant priming mechanism undergoing at each planted treatment. The data

indicates that, exudate composition is influenced by the plants N status. Under N-deficiency plants exudate more organic acids and less energy rich compounds, thus prevailing the "N-mining" priming mechanism. When supplied with N, the plants release a more compound diverse exudate, leading to the dominance of the "microbial stoichiometry" mechanism. The different dominant mechanisms indicate that different microbial communities are benefited depending on the plant N status. As the N-deficient plants affected more the physicochemical characteristics of the soil, and may have increased the population of K-strategists, a global scenario in which plants under N deficiency induce the mineralization of mineral associated C is plausible.

These results are to our knowledge, the first demonstration of different priming mechanisms due to plant N-status. Our work, reflects the importance of careful nutrient management in forest plantations, and highlights the possibility of higher C mineralization in N-deficient forests. We recommend that future studies, take into account other important nutrients such as P, K.

FIGURES

Table 1. Mean Leaf-$_{SPAD\ Index}$, new shoot and root dry mass and root:shoot ratio of Eucalypt seedlings as affected by N supply. Means followed by the same case letter do not differ by F-test ($p<0.05$).

Parameter	+ N		- N	
	Shoot	Root	Shoot	Root
Leaf-$_{SPAD\ Index}$	41.33±1.76 a	-	27.33±1.20 b	-
Dry mass (g)	2.01±0.14 a	0.42±0.04 A	1.19±0.04 b	0.41±0.02 A
Root:Shoot	0.21±0.02 b		0.35±0.05 a	

+N is the fertilized treatment and -N the unfertilized one.

Table 2. Mean root traits estimated at the end of the experimental period for Eucalypt seedling sunder distinct N-supply computed by the GiaRoots Software. Means followed by the same case letter do not differ by F-test ($p<0.05$).

Root traits	+ N	- N	p-value
Root average width (mm)	3.77 A	2.84 A	0.087
Root length (cm)	900.64 B	1814.34 A	0.049
Root surface area (cm^2)	94.36 B	178.69 A	0.031

+N is the fertilized treatment and -N the unfertilized one.

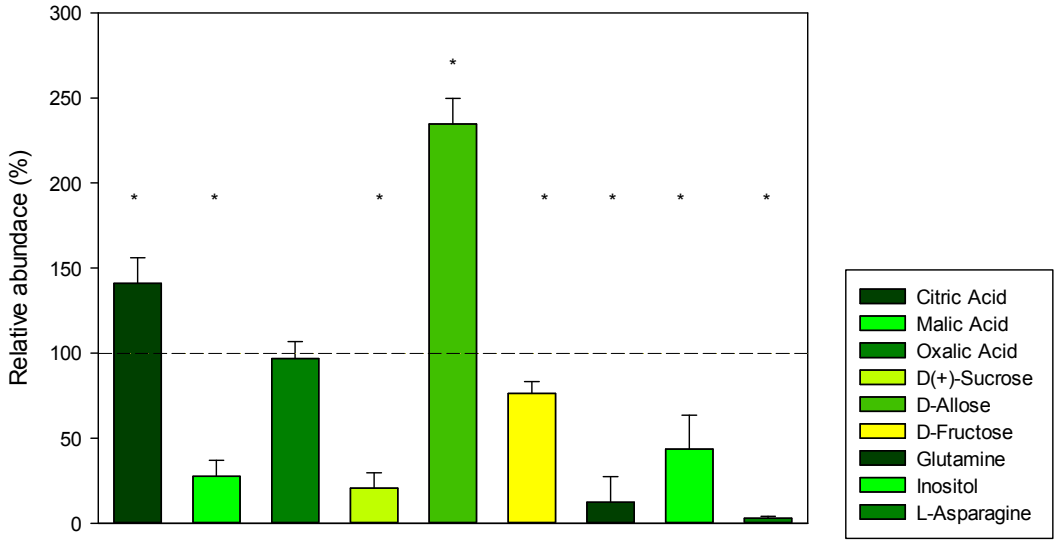

Figure 1. Metabolic profiling of the lower compartment roots from – N planted treatment. The dashed line indicates the relative abundance of each compound in the +N planted treatment. Values differing from the +N planted treatment denote a treatment induced change, signed by an asterisk (F-test, $p < 0.05$). Values are shown as relative abundance of each compound to the same compound in the +N planted treatment ± s.e.m. (n=3).

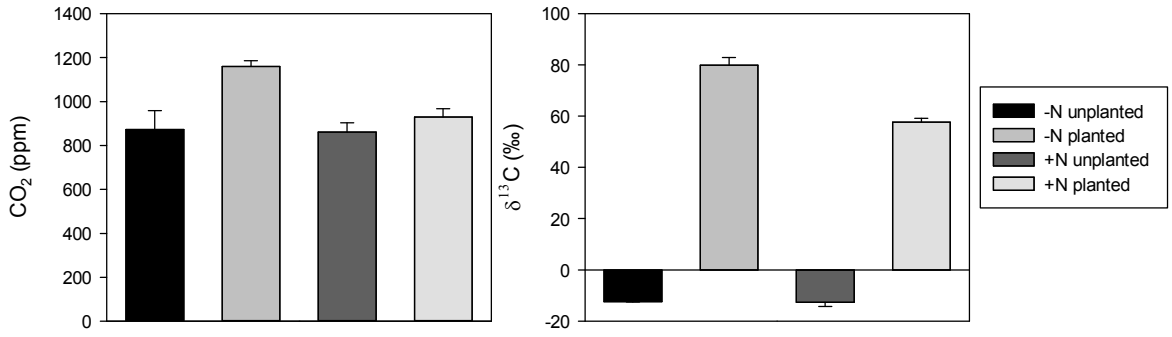

Figure 2. (a) Mean soil CO_2 concentrations and (b) δ^{13}C-CO2 of the rhizospheric soil air, 16 hours after a pulse with ^{13}C enriched CO_2 at the end of the experimental period. Values differing from the control (-Pl/-N) denote a treatment induced change, signed by an asterisk (F-test, $p < 0.05$). Values are shown as means ± s.e.m. (n=3).

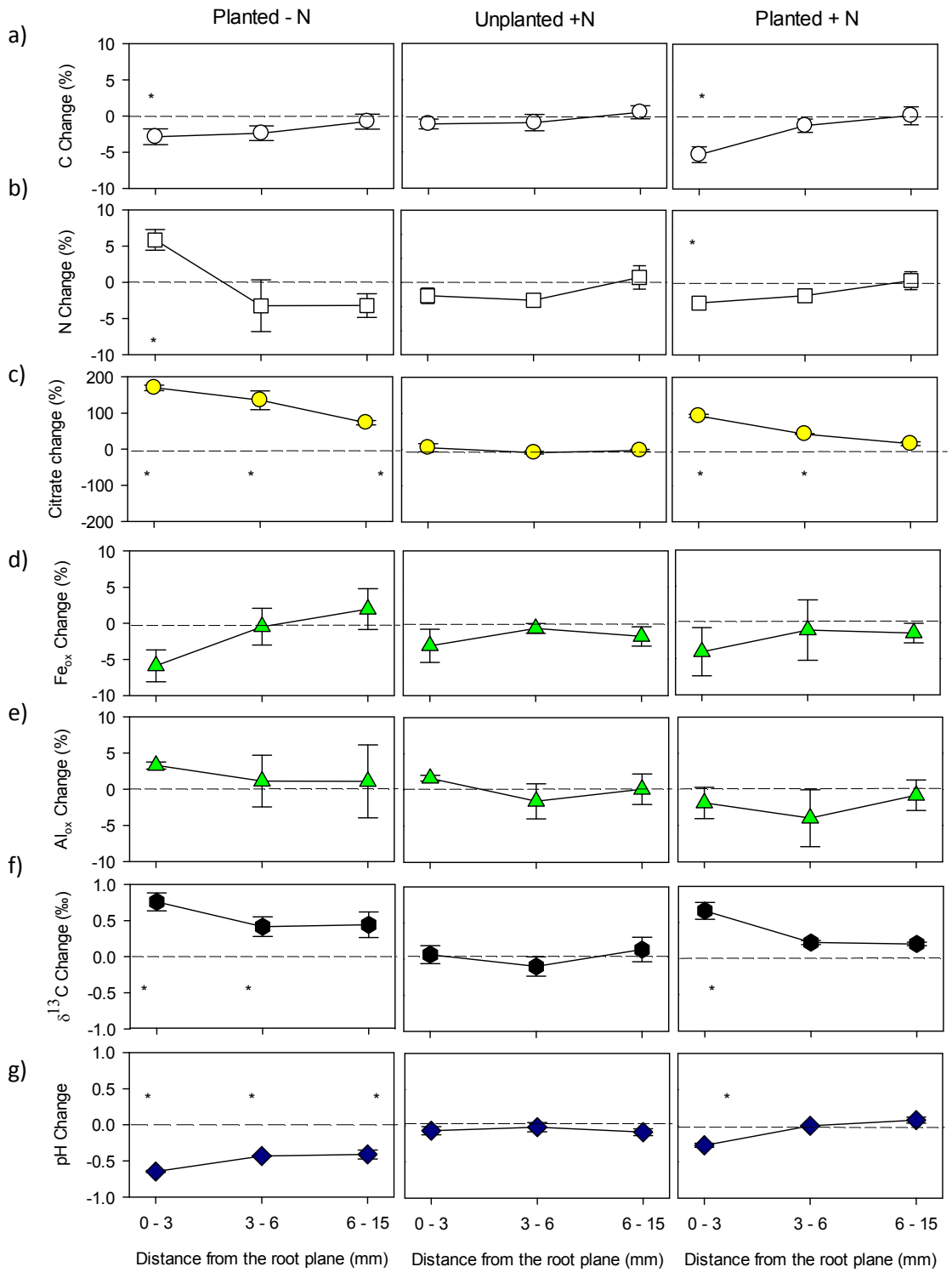

Figure 3. Induced effects of *Eucalyptus spp.* exudation on the MAOM's C, N, $\delta^{13}C$ and soil solution Citrate concentration. (a, b, f and c), protective mineral phases and in soil pH (d, e and g), presented as function of distance from the root plane. Effects were calculated as the

percentage difference between concentrations in the treatment and the control (-N unplanted treatment) or as diference of the treatment to the control value. Values differing from that of the dashed line denote a treatment induced change, asterisks sign a significant change from the control (two way ANOVA, followed by Dunnet's test $p < 0.05$). Values are shown as means ± s.e.m. (n=3).

Table 3. Relative changes in CO_2 (m/z 44) evolution from the MAOM fraction from plants fertilized (+N) and not (-N) with Nitrogen. Percentages are relative to the CO_2 evolution of the no plant control.

Temperature Range °C	+Pl/+N	+Pl/-N	+Pl/+N	+Pl/-N
	Distance from the Root Plane (mm)			
	0 - 3		3 - 6	
0 - 155	-32%	-37%	14%	-16%
155 - 320	-15%	-13%	-9%	-19%
320 - 500	-3%	-24%	6%	0%

+Pl is the planted treatment, -Pl the unplanted one, +N the N-fertilized treatment and -N the N-unfertilized one.

Table 4. Changes in the goethite mineralogy assessed by synchrotron based XRD.

Treatment	Mineral	hkl	d (Å)	FWHM
-Pl/-N	Goethite	1 0 1	4.1580	0.826
+Pl/-N			4.1314	0.531
-Pl/+N			4.1530	0.826
+Pl/+N			4.1492	0.732

+Pl is the planted treatment, -Pl the unplanted one, +N the fertilized treatment and -N the unfertilized one.
FWHM: Full width at half maximum

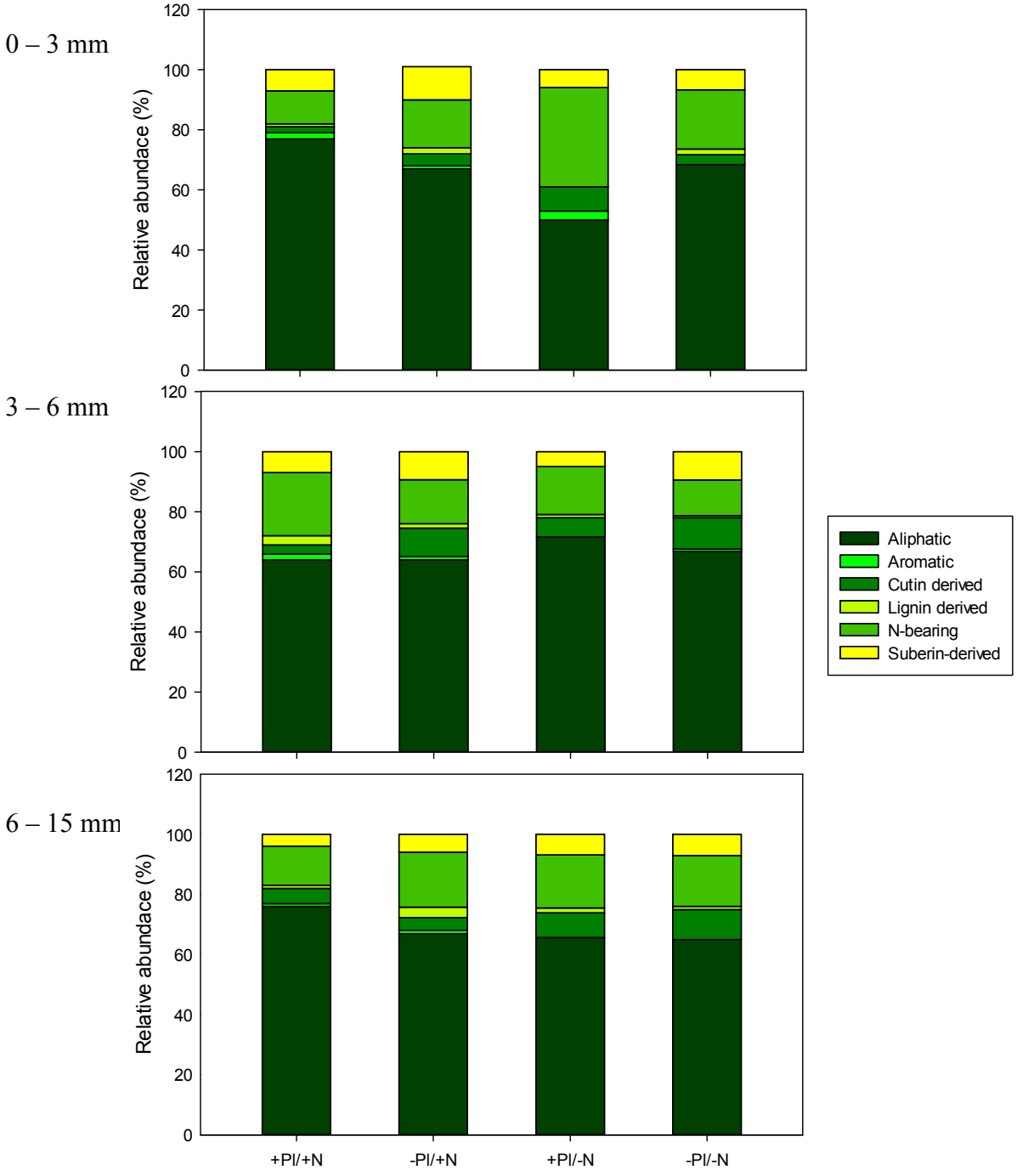

Figure 4. Relative abundance of chemical compound groups in the mineral associated organic matter fraction in the distance 0 – 3, 3 – 6 and 6 – 1.5 mm from the root plane. +P & -P denotes the planted and unplanted treatments respectively. +N & -N denote the fertilized and unfertilized treatments.

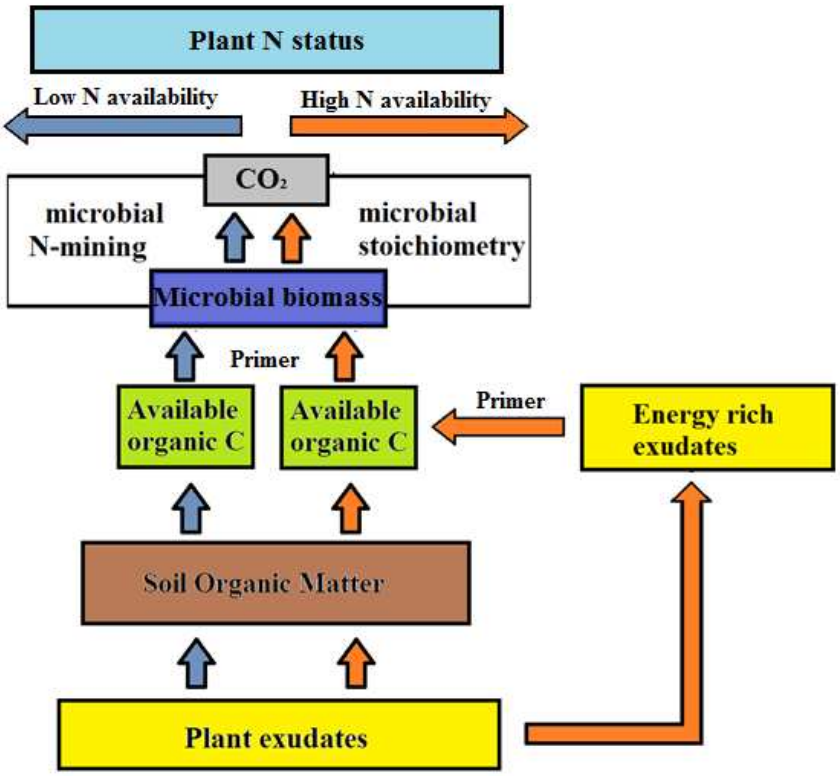

Figure 5. Possible dominant mechanisms of nutrient-driven priming effect in the planted treatments under N deficiency and high N availability. The blue lines show fluxes controlled by native microbial populations (K-strategists) and red lines show fluxes controlled by opportunistic microbial communities (r-strategists). Adapted from (Chen et al., 2014).

REFERENCES

Amundson, R., Berhe, A.A., Hopmans, J.W., Olson, C., Sztein, A.E., Sparks, D.L., 2015. Soil science. Soil and human security in the 21st century. Science (New York, N.Y.) 348, 1261071. doi:10.1126/science.1261071

Bonan, G.B., 2008. Forests and climate change: forcings, feedbacks, and the climate benefits of forests. Science 320, 1444–1449. doi:10.1126/science.1155121

Cambardella, C.A., Elliott, E.T., 1992. Particulate Soil Organic-Matter Changes across a Grassland Cultivation Sequence. Soil Science Society of America Journal 56, 777. doi:10.2136/sssaj1992.03615995005600030017x

Carvalhais, L.C., Dennis, P.G., Fedoseyenko, D., Hajirezaei, M.R., Borriss, R., Von Wir??n, N., 2011. Root exudation of sugars, amino acids, and organic acids by maize as affected by nitrogen, phosphorus, potassium, and iron deficiency. Journal of Plant Nutrition and Soil Science 174, 3–11. doi:10.1002/jpln.201000085

Chen, R., Senbayram, M., Blagodatsky, S., Myachina, O., Dittert, K., Lin, X., Blagodatskaya, E., Kuzyakov, Y., 2014. Soil C and N availability determine the priming effect: Microbial N mining and stoichiometric decomposition theories. Global Change Biology 20, 2356–2367. doi:10.1111/gcb.12475

del Rio, J.., McKinney, D.., Knicker, H., Nanny, M.., Minard, R.., Hatcher, P.., 1998. Structural characterization of bio- and geo-macromolecules by off-line thermochemolysis with tetramethylammonium hydroxide. Journal of Chromatography A 823, 433–448. doi:10.1016/S0021-9673(98)00268-4

Dijkstra, F.A., Carrillo, Y., Pendall, E., Morgan, J.A., 2013. Rhizosphere priming: A nutrient

perspective. Frontiers in Microbiology 4. doi:10.3389/fmicb.2013.00216

Drake, J.E., Darby, B.A., Giasson, M.A., Kramer, M.A., Phillips, R.P., Finzi, A.C., 2013. Stoichiometry constrains microbial response to root exudation-insights from a model and a field experiment in a temperate forest. Biogeosciences 10, 821–838. doi:10.5194/bg-10-821-2013

Farrar, J., Hawes, M., Jones, D., Lindow, S., 2003. How roots control the flux of carbon to the rhizosphere. Ecology. doi:10.1890/0012-9658(2003)084[0827:HRCTFO]2.0.CO;2

Fitz, W.J., Wenzel, W.W., Wieshammer, G., Isteni??, B., 2003. Microtome sectioning causes artifacts in rhizobox experiments. Plant and Soil 256, 455–462. doi:10.1023/A:1026173613947

Furrer, G., Stumm, W., 1986. The coordination chemistry of weathering: I. Dissolution kinetics of [delta]-Al2O3 and BeO. Geochimica et Cosmochimica Acta 50, 1847–1860. doi:10.1016/0016-7037(86)90243-7

Galkovskyi, T., Mileyko, Y., Bucksch, A., Moore, B., Symonova, O., Price, C.A., Topp, C.N., Iyer-Pascuzzi, A.S., Zurek, P.R., Fang, S., 2012. GiA Roots: software for the high throughput analysis of plant root system architecture. BMC Plant Biology 12, 1.

He, Y., Trumbore, S.E., Torn, M.S., Harden, J.W., Vaughn, L.J.S., Allison, S.D., Randerson, J.T., 2016. Radiocarbon constraints imply reduced carbon uptake by soils during the 21st century. Science 353, 1419–1424. doi:10.1126/science.aad4273

Heimann, M., Reichstein, M., 2008. Terrestrial ecosystem carbon dynamics and climate feedbacks. Nature 451, 289–292. doi:10.1038/nature06591

Hermans, C., Hammond, J.P., White, P.J., Verbruggen, N., 2006. How do plants respond to nutrient shortage by biomass allocation? Trends in Plant Science 11, 610–617. doi:10.1016/j.tplants.2006.10.007

Hungate, B.A., 2003. Nitrogen and Climate Change. Science 302, 1512–1513. doi:10.1126/science.1091390

Jobbágy, E.G., Jackson, R.B., 2000. the Vertical Distribution of Soil Organic Carbon and Its. Ecological Applications 10, 423–436. doi:10.1890/1051-0761(2000)010[0423:TVDOSO]2.0.CO;2

Jones, D.L., Nguyen, C., Finlay, R.D., 2009. Carbon flow in the rhizosphere: Carbon trading at the soil-root interface. Plant and Soil 321, 5–33. doi:10.1007/s11104-009-9925-0

Jourdan, C., Silva, E. V., Gonçalves, J.L.M., Ranger, J., Moreira, R.M., Laclau, J.P., 2008. Fine root production and turnover in Brazilian Eucalyptus plantations under contrasting nitrogen fertilization regimes. Forest Ecology and Management 256, 396–404. doi:10.1016/j.foreco.2008.04.034

Kallenbach, C.M., Grandy, A., Frey, S.D., 2016. Direct evidence for microbial-derived soil organic matter formation and its ecophysiological controls. Nature Communications in revisio, 1–10. doi:10.1038/ncomms13630

Kammann, C., Grünhage, L., Jäger, H.J., 2001. A new sampling technique to monitor concentrations of CH4, N2O and CO2 in air at well-defined depths in soils with varied water potential. European Journal of Soil Science 52, 297–303. doi:10.1046/j.1365-2389.2001.00380.x

Koch, K., 2004. Sucrose metabolism: Regulatory mechanisms and pivotal roles in sugar

sensing and plant development. Current Opinion in Plant Biology 7, 235–246. doi:10.1016/j.pbi.2004.03.014

Kuzyakov, Y., 2002. Review: Factors affecting rhizosphere priming effects. Journal of Plant Nutrition and Soil Science 165, 382. doi:10.1002/1522-2624(200208)165:4<382::AID-JPLN382>3.0.CO;2-#

Kuzyakov, Y., Blagodatskaya, E., 2015. Microbial hotspots and hot moments in soil: Concept & review. Soil Biology and Biochemistry 83, 184–199. doi:10.1016/j.soilbio.2015.01.025

Lisec, J., Schauer, N., Kopka, J., Willmitzer, L., Fernie, A.R., 2006. Gas chromatography mass spectrometry-based metabolite profiling in plants. Nat Protoc 1, 387–396. doi:10.1038/nprot.2006.59

Machado, D.N., Novais, R.F., da Silva, I.R., Loureiro, M.E., Milagres, J.J., Soares, E.M.B., 2011. Enriquecimento e alocação de 13C em plantas de eucalipto. Revista Brasileira de Ciencia Do Solo 35, 857–866. doi:10.1590/S0100-06832011000300020

Marschner, H., Kirkby, E. a, Cakmak, I., 1996. Effect of mineral nutritional status on shoot-root partitioning of photoassimilates and cycling of mineral nutrients. Journal of Experimental Botany 47 Spec No, 1255–1263. doi:10.1093/jxb/47.Special_Issue.1255

Meier, I.C., Finzi, A.C., Phillips, R.P., 2017. Root exudates increase N availability by stimulating microbial turnover of fast-cycling N pools. Soil Biology and Biochemistry 106, 119–128. doi:10.1016/j.soilbio.2016.12.004

Ostonen, I., Püttsepp, Ü., Biel, C., Alberton, O., Bakker, M.R., Lõhmus, K., Majdi, H., Metcalfe, D., Olsthoorn, A.F.M., Pronk, A., Vanguelova, E., Weih, M., Brunner, I.,

2007. Specific root length as an indicator of environmental change. Plant Biosystems - An International Journal Dealing with All Aspects of Plant Biology 141, 426–442. doi:10.1080/11263500701626069

Pansu, M., Gautheyrou, J., 2006. Handbook of soil analysis: Mineralogical, organic and inorganic methods, Handbook of Soil Analysis: Mineralogical, Organic and Inorganic Methods. doi:10.1007/978-3-540-31211-6

Paterson, E., Gebbing, T., Abel, C., Sim, A., Telfer, G., 2007. Rhizodeposition shapes rhizosphere microbial community structure in organic soil. The New Phytologist 173, 600–610. doi:10.1111/j.1469-8137.2006.01931.x

Paul, M.J., Driscoll, S.P., 1997. Sugar repression of photosynthesis: the role of carbohydrates in signalling nitrogen deficiency through source:sink imbalance. Plant, Cell and Environment 20, 110–116. doi:10.1046/j.1365-3040.1997.d01-17.x

Pérez, D.V., de Campos, R.C., Novaes, H.B., 2002. Soil solution charge balance for defining the speed and time of centrifugation of two Brazilian soils. Communications in Soil Science and Plant Analysis 33, 2021–2036. doi:10.1081/CSS-120005746

Philippot, L., Raaijmakers, J.M., Lemanceau, P., van der Putten, W.H., 2013. Going back to the roots: the microbial ecology of the rhizosphere. Nature Reviews. Microbiology 11, 789–99. doi:10.1038/nrmicro3109

Rasse, D.P., Rumpel, C., Dignac, M.F., 2005. Is soil carbon mostly root carbon? Mechanisms for a specific stabilisation, in: Plant and Soil. pp. 341–356. doi:10.1007/s11104-004-0907-y

Rumpel, C., Kögel-Knabner, I., 2011. Deep soil organic matter-a key but poorly understood

component of terrestrial C cycle. Plant and Soil 338, 143–158. doi:10.1007/s11104-010-0391-5

Shang, C., Zelazny, L.W., 2008. Selective Dissolution Techniques for Mineral Analysis of Soils and Sediments, in: Methods of Soil Analysis Part 5—Mineralogical Methods, SSSA Book Series SV - 5.5. Soil Science Society of America, Madison, WI, pp. 33–80. doi:10.2136/sssabookser5.5.c3

Silva, I.R., Novais, R.F., Jham, G.N., Barros, N.F., Gebrim, F.O., Nunes, F.N., Neves, J.C.L., Leite, F.P., 2004. Responses of eucalypt species to aluminum: the possible involvement of low molecular weight organic acids in the Al tolerance mechanism. Tree Physiology 24, 1267–1277. doi:10.1093/treephys/24.11.1267

Stape, J.L., Binkley, D., Ryan, M.G., 2004. Eucalyptus production and the supply, use and efficiency of use of water, light and nitrogen across a geographic gradient in Brazil. Forest Ecology and Management 193, 17–31. doi:10.1016/j.foreco.2004.01.020

Trumbore, S., Brando, P., Hartmann, H., Gauthier, S., Bernier, P., Kuuluvainen, T., Shvidenko, A.Z., Schepaschenko, D.G., 2015. Forest health and global change. Science (New York, N.Y.).

Tschoep, H., Gibon, Y., Carillo, P., Armengaud, P., Szecowka, M., Nunes-Nesi, A., Fernie, A.R., Koehl, K., Stitt, M., 2009. Adjustment of growth and central metabolism to a mild but sustained nitrogen-limitation in Arabidopsis. Plant, Cell and Environment 32, 300–318. doi:10.1111/j.1365-3040.2008.01921.x

Wenzel, W.W., Wieshammer, G., Fitz, W.J., Puschenreiter, M., 2001. Novel rhizobox design to assess rhizosphere characteristics at high spatial resolution. Plant and Soil 237, 37–

45. doi:10.1023/A:1013395122730

Wieder, W.R., Cleveland, C.C., Smith, W.K., Todd-Brown, K., 2015. Future productivity and carbon storage limited by terrestrial nutrient availability. Nature Geoscience 8, 441-U35. doi:10.1038/ngeo2413

Zinder, B., Furrer, G., Stumm, W., 1986. The coordination chemistry of weathering: II. Dissolution of Fe(III) oxides. Geochimica et Cosmochimica Acta 50, 1861–1869. doi:10.1016/0016-7037(86)90244-9

SUPPLEMENTARY MATERIAL

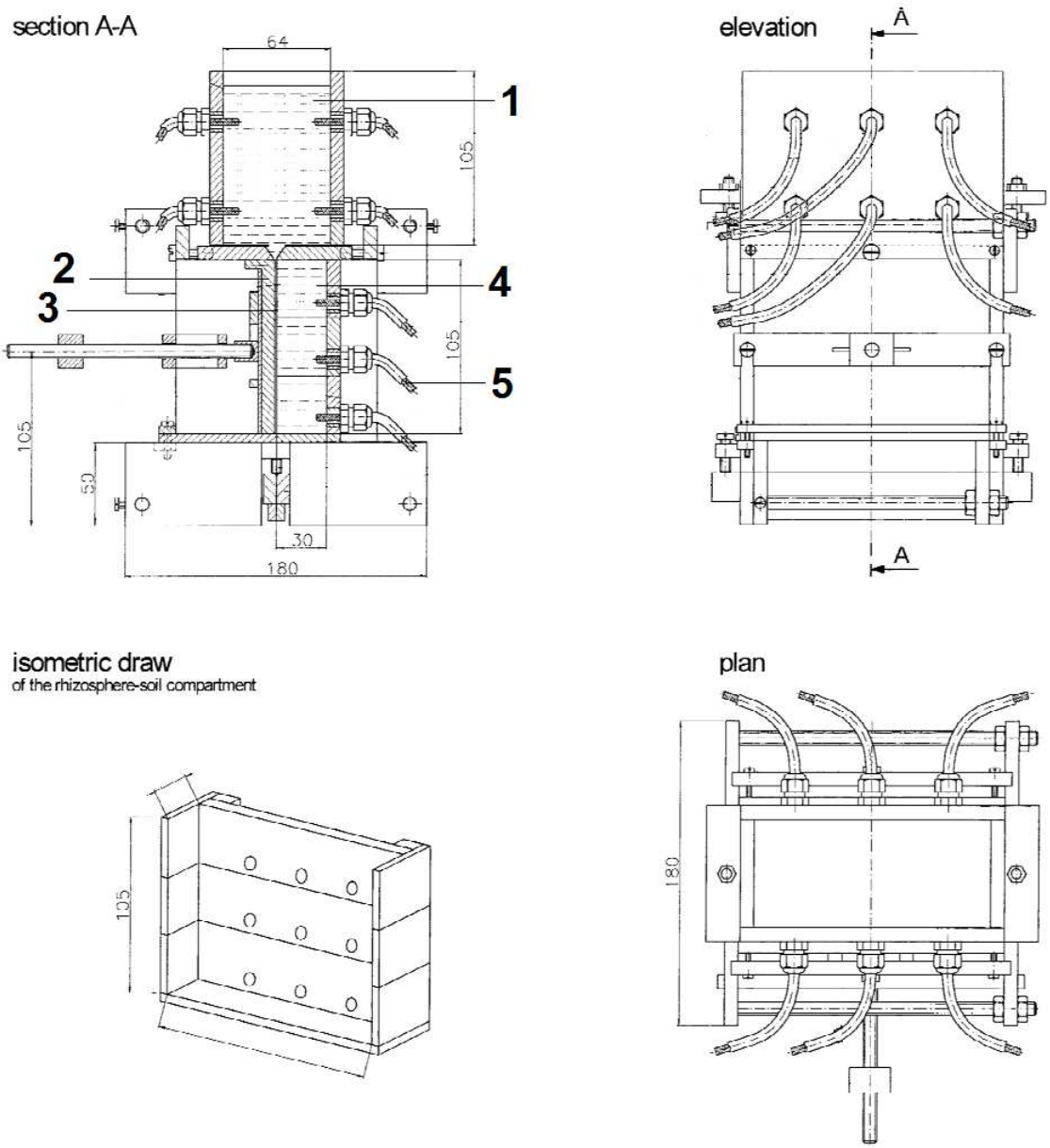

Supplementary Figure 1. Rhizobox design and cross sections. Legend: (1) soil–plant compartment; (2) transparent acrylic wall; (3) nylon membrane (meshwidth 5 µm); (4) rhizosphere soil compartment; (5) irrigation wicks (fiber glass, Fiberseals, diameter 5mm).

Supplementary Table 1. Modified Clark Solution used for the rhizobox experiment.

Macronutrients (mmol/L)						
Ca	K	$N\text{-}NH_4$	$N\text{-}NO_3$	Mg	S	P
2.6	1.8	3.5	3.5	0.6	0.6	0.138
		$^{15}N\text{-}NH_4$				
		0.01				
Micronutrients (mmol/L)						
Fe	B	Zn	Cu	Mn	Mo	
0.09	0.019	0.02	0.0005	0.007	0.0006	
Others						
Al						
0.05						

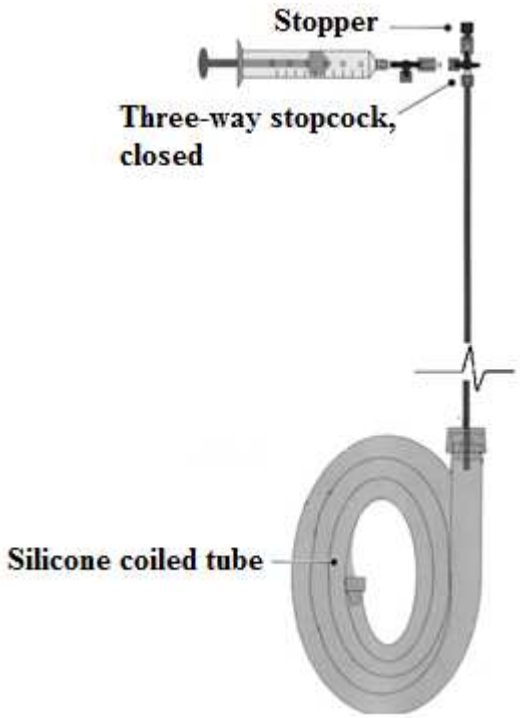

Supplementary Figure 2. Soil-air gas sampler. The flat silicone coil is fixed with tape (not shown) to maintain the flat form. The end of the silicone coil was closed with a plastic shutter.

Supplementary Table 2. Two-way ANOVA results for physico-chemical properties of the MAOM fraction (total organic C, $\delta^{13}C$, Fe-oxalate and Al-oxalate and total N), Citrate concentration in the soil solution and soil pH_{H2O}

Distance	Treatment	TOC	$\delta^{13}C$	pH	Fe-Ox	Al-Ox	Citrate	N
		p Value						
0 - 3	Nitrogen	0.01	0.77	0.00	0.32	0.29	0.00	0.00
	Plant	0.00	0.01	0.00	0.01	0.19	0.00	0.49
	Plant x Nitrogen	0.47	0.76	0.00	0.00	0.53	0.00	0.00
3 - 6	Nitrogen	0.90	0.09	0.00	0.84	0.58	0.00	0.21
	Plant	0.10	0.29	0.00	0.95	0.53	0.00	0.30
	Plant x Nitrogen	0.20	0.15	0.00	0.95	0.82	0.01	0.53
6 - 15	Nitrogen	0.32	0.18	0.02	0.36	0.55	0.00	0.32
	Plant	0.98	0.01	0.25	0.39	0.96	0.00	0.98
	Plant x Nitrogen	0.54	0.52	0.00	0.67	0.27	0.00	0.54

a)

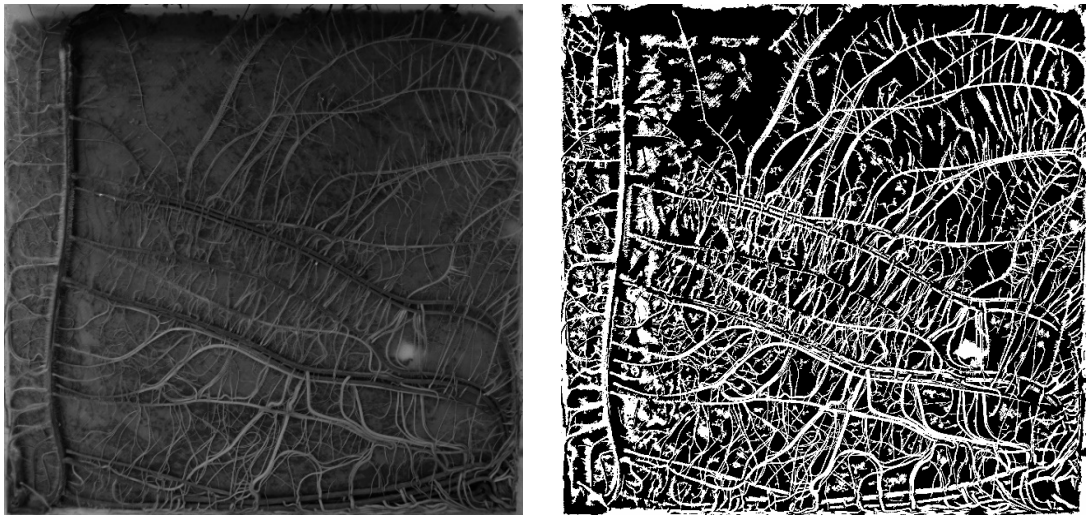

b)

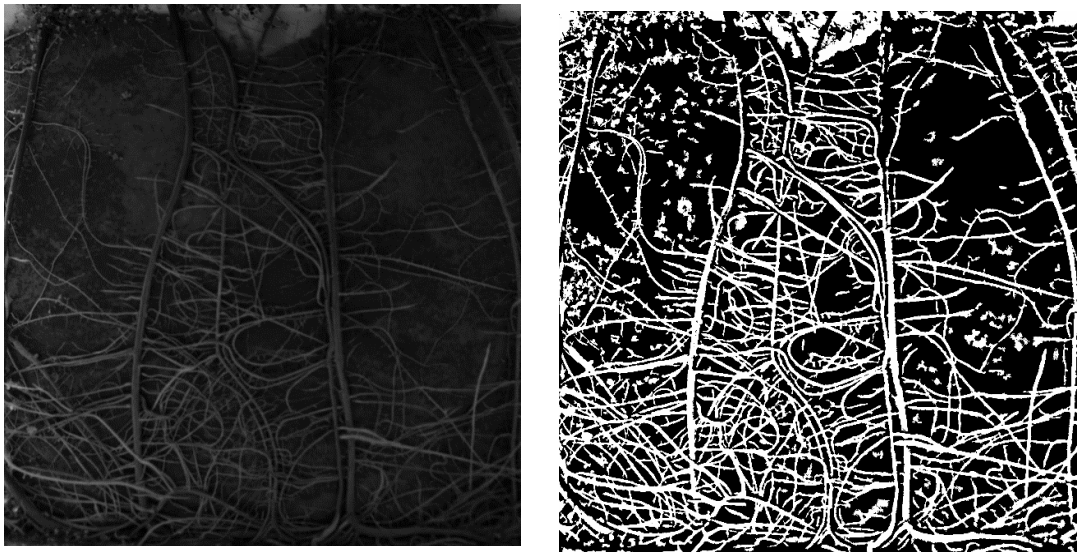

Supplementary Figure 3. Cropped and thresholded image of an (a) N-unfertilized treatment and a N-fertilized treatment, after data treatment in the GiaRoots software.

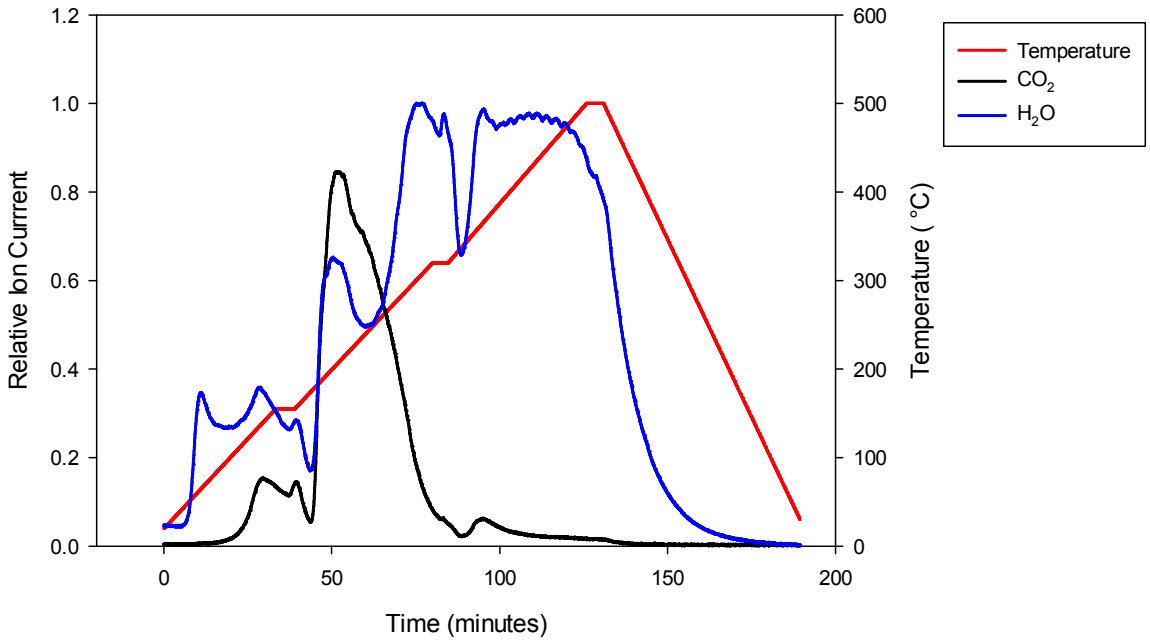

Supplementary Figure 4. CO_2 (m/z 44) and H_2O (m/z 18) evolution of the MAOM fraction along the heat ramp during thermal decomposition.

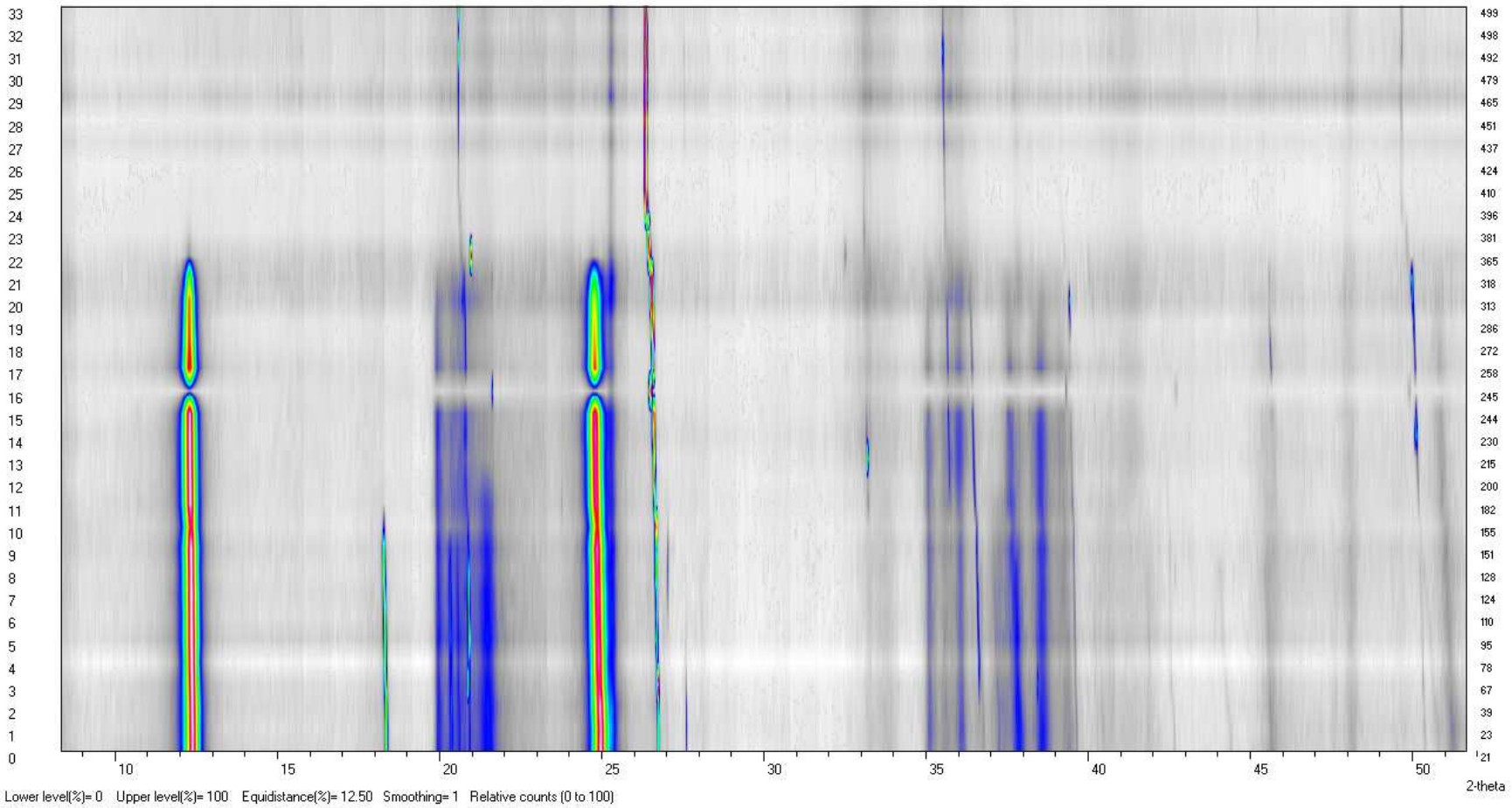

Supplementary Figure 5 Synchrotron-based X-ray diffraction pattern evolution during the thermal decomposition of the MAOM fraction. Main features included are: (Kaolinite: 12 °2θ, Gibbsite: 18 °2θ, Goethite: 21 °2θ and Quartz: 27 °2θ).

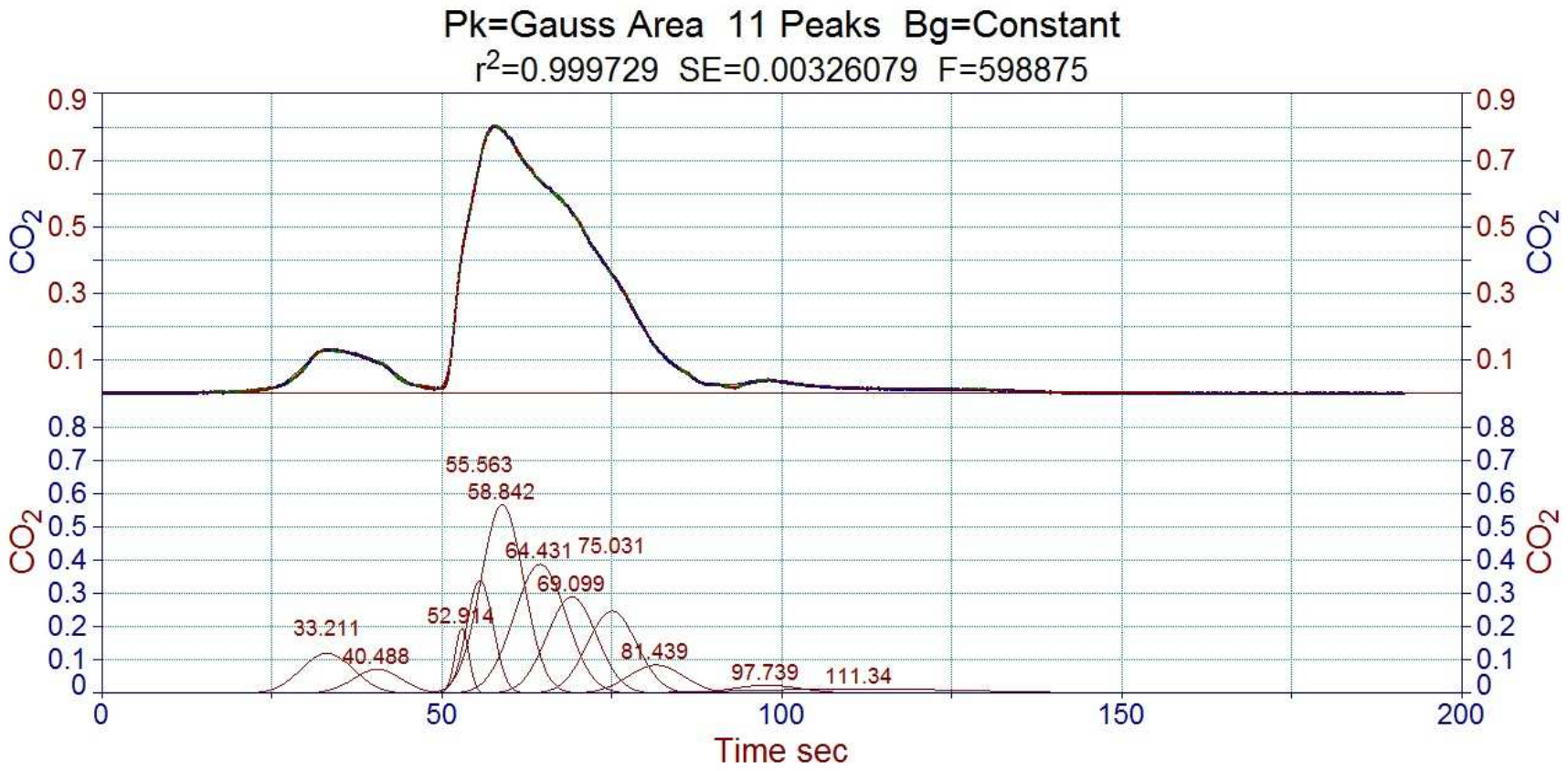

Supplementary Figure 6: Deconvoluted signal of the CO_2 evolution of the MAOM fraction during thermal decomposition.

Supplementary Table 3. Percentages of each chemical group to the total composition assessed by TMAH-GC/MS. Statistically significant values are denoted by diferent upper case letter (two way ANOVA, followed by LSD test $p < 0.05$). Values are shown as means (n=3).

Dist.	Treatment.	Group					
		Aliph.	Aromatic	Cutin derived	Lignin Derived	N-bearing	Suberin derived
0 - 3	+P/+N	77%^{A}	2%	2%	1%	11%^{C}	7%^{B}
	-P/+N	67%^{B}	1%	4%	2%	16%^{B}	11%^{AB}
	+P/-N	50%^{C}	3%	8%	0%	33%^{A}	6%^{B}
	-P/-N	68%^{B}	0%	3%	2%	20%^{B}	7%^{B}
3 – 6	+P/+N	64%^{B}	2%	3%	3%	21%^{A}	7%
	-P/+N	64%^{B}	1%	9%	2%	15%^{B}	9%
	+P/-N	72%^{A}	0%	6%	1%	16%^{B}	5%
	-P/-N	67%^{B}	1%	10%	1%	12%^{B}	9%
6 -15	+P/+N	76%^{A}	1%	5%	1%	13%	4%
	-P/+N	67%^{B}	1%	4%	3%	18%	6%
	+P/-N	66%^{B}	0%	8%	2%	18%	7%
	-P/-N	65%^{B}	0%	10%	1%	17%	7%

Supplementary Table 4. Main products released from off line Thermochemolysis (TMAH-GC/MS), within the first distance (0 – 3 mm).

Name	Origin	+Pl/+N	-Pl/+N	+Pl/-N	-Pl/-N
1-Docosanol, methyl ether	Aliphatic	X	X	X	X
1-Heneicosanol	Aliphatic	X			
1-Hentetracontanol	Aliphatic	X			
1-Heptacosanol	Aliphatic	X	X		X
1-Hexacosanol	Aliphatic			X	
1-Hexanol, 5-methyl-2-(1-methylethyl)-	Aliphatic			X	
1-Triacontanol	Aliphatic	X		X	
2,2-Dimethyloctadecane	Aliphatic	X			
2-Isopropyl-5-methyl-1-heptanol	Aliphatic			X	
5,5-Diethylheptadecane	Aliphatic	X			
9-Octadecenoic acid, methyl ester, (E)-	Aliphatic			X	
Cyclopropaneoctanoic acid, 2-[[2-[(2-ethylcyclopropyl)methyl]cyclopropyl]methyl]-, methyl ester	Aliphatic	X			
Decane, 2,3,4-trimethyl-	Aliphatic		X		
Decane, 3,3,8-trimethyl-	Aliphatic		X		
Docosanoic acid, methyl ester	Aliphatic			X	

Dodecane	Aliphatic			X	
Eicosane	Aliphatic	X	X	X	X
Heptadecane	Aliphatic	X	X	X	X
Heptadecane, 8-methyl-	Aliphatic	X	X	X	X
Hexacosane	Aliphatic		X	X	
Hexacosanoic acid, methyl ester	Aliphatic	X	X	X	X
Hexane, 2,4,4-trimethyl-	Aliphatic	X			
Hexyl octyl ether	Aliphatic		X		
Methyl 18-methylnonadecanoate	Aliphatic	X	X	X	X
n-Nonadecanol-1	Aliphatic	X			
Nonane, 5-(1-methylpropyl)-	Aliphatic		X		
Nonane, 5-(2-methylpropyl)-	Aliphatic		X	X	
Nonane, 5-methyl-5-propyl-	Aliphatic	X	X		
n-Tetracosanol-1	Aliphatic	X		X	
Octacosane	Aliphatic				X
Octacosanoic acid, methyl ester	Aliphatic		X	X	X
Octadecane	Aliphatic			X	
Octane, 4-methyl-	Aliphatic	X			
Oleyl alcohol, methyl ether	Aliphatic	X			X
Oxirane, tetradecyl-	Aliphatic	X			
Pentacosanoic acid, methyl ester	Aliphatic		X		X
Pentadecanoic acid, 14-methyl-, methyl ester	Aliphatic			X	
Pentane, 1-butoxy-	Aliphatic	X			
Pentane, 3,3-dimethyl-	Aliphatic	X	X		
Pentatriacontane	Aliphatic		X	X	X
Tetracontane	Aliphatic	X	X	X	
Tetracosanoic acid, methyl ester	Aliphatic	X		X	X
Tetradecane, 2,2-dimethyl-	Aliphatic		X		X
Tetrapentacontane	Aliphatic				X
Triacontanoic acid, methyl ester	Aliphatic		X		
2-Cyclopenten-1-one, 3-ethyl-2-hydroxy-	Aromatic			X	
Phenol, 2,4-bis(1,1-dimethylethyl)-	Aromatic	X	X		
Phthalic acid, butyl 6-methylhept-2-yl ester	Aromatic			X	
Phthalic acid, butyl dodecyl ester	Aromatic	X			
Phthalic acid, hept-3-yl isobutyl ester	Aromatic			X	
Hexadecanoic acid, 2-hydroxyethyl ester	Cutin Derived	X	X	X	
n-Hexadecanoic acid	Cutin Derived			X	
Benzoic acid, 4-hydroxy-3-methoxy-, methyl ester	Lignin Derived	X	X		X
13-Docosenamide, (Z)-	N-bearing		X		

1H-Indole, 1,2,3-trimethyl-	N-bearing			X	
2,5-Pyrrolidinedione, 1-methyl-	N-bearing			X	
2-Amino-5,6-dihydro-4,4,6-trimethyl-4H-1,3-oxazine	N-bearing			X	
3-Dimethylaminoanisole	N-bearing			X	
5,10-Diethoxy-2,3,7,8-tetrahydro-1H,6H-dipyrrolo[1,2-a:1',2'-d]pyrazine	N-bearing	X	X	X	X
9H-Purin-6-amine, N,N,9-trimethyl-	N-bearing	X		X	X
Caffeine	N-bearing			X	X
Hexadecanamide	N-bearing			X	
Morpholine, 4-acetyl-	N-bearing	X	X		
N,N-Dimethyldodecanamide	N-bearing	X			X
N-[6-[N-Aziridyl]-3-aza-3-hexenyl]morpholine	N-bearing			X	
N-Formylmorpholine	N-bearing	X	X		
Octadecanamide	N-bearing	X	X		X
Octanamide, N,N-dimethyl-	N-bearing		X		
Piperazine, 1-methyl-	N-bearing				X
Piperazine-2,5-dione, 1,4-dimethyl-3,3'-bis-	N-bearing				X
Methyl stearate	Suberin Derived	X	X	X	X
Octadecanoic acid	Suberin Derived	X	X	X	X
2,2,4-Trimethyl-1,3-pentanediol diisobutyrate	Unk.	X	X		X
6-[2-Hexahydroazepino-1-hydroxyethyl]-8-methyl-2-p-methylphenylquinoline	Unk.				
l-(+)-Ascorbic acid 2,6-dihexadecanoate	Unk.	X	X	X	X
Oxirane, decyl-	Unk.	X			
Oxirane, hexadecyl-	Unk.	X			
Pentanoic acid, 5-hydroxy-, 2,4-di-t-butylphenyl esters	Unk.				X

Supplementary Table 5. Main products released from off line Thermochemolysis (TMAH-GC/MS), within the second distance (3 – 6 mm).

Name	Origin	+Pl/+N	-Pl/+N	+Pl/-N	-Pl/-N
1-Butanol, 2,3-dimethyl-	Aliphatic	X			
1-Decanol, 2-hexyl-	Aliphatic	X			
1-Docosanol, methyl ether	Aliphatic	X	X	X	X
1-Heneicosanol	Aliphatic		X		
1-Hentetracontanol	Aliphatic	X			
1-Heptacosanol	Aliphatic	X	X	X	X
1-Hexacosanol	Aliphatic			X	
1-Hexanol, 5-methyl-2-(1-methylethyl)-	Aliphatic		X		
1-Triacontanol	Aliphatic		X	X	
4,4-Dimethyl octane	Aliphatic	X			
9-Hexadecenoic acid, methyl ester, (Z)-	Aliphatic			X	
9-Octadecenoic acid, methyl ester, (E)-	Aliphatic				X
Cyclopropaneoctanoic acid, 2-octyl-, methyl ester	Aliphatic	X			
Decane, 5-propyl-	Aliphatic	X			
Docosanoic acid, methyl ester	Aliphatic			X	
Dodecane, 4-methyl-	Aliphatic	X			
Dotriacontane	Aliphatic		X		
Eicosane	Aliphatic	X	X	X	X
Ethanone, 1-(3-methyloxiranyl)-	Aliphatic	X			
Heneicosanoic acid, methyl ester	Aliphatic			X	
Heptadecane	Aliphatic		X	X	X
Heptadecane, 3-methyl-	Aliphatic		X		
Heptadecane, 7-methyl-	Aliphatic	X			
Heptadecane, 8-methyl-	Aliphatic	X	X		X
Heptane, 2,3-dimethyl-	Aliphatic		X		
Heptane, 3,3,4-trimethyl-	Aliphatic	X			
Hexacosane	Aliphatic	X	X		X
Hexacosanoic acid, methyl ester	Aliphatic	X			X
Hexadecane, 2,6,11,15-tetramethyl-	Aliphatic	X			
Methyl 18-methylnonadecanoate	Aliphatic	X	X	X	X
Morpholine, 4-acetyl-	Aliphatic	X			
Nonane, 2,6-dimethyl-	Aliphatic	X			
Nonane, 5-(1-methylpropyl)-	Aliphatic	X			

n-Tetracosanol-1	Aliphatic	X		X	X
Octacosane	Aliphatic			X	
Octacosanoic acid, methyl ester	Aliphatic	X		X	X
Oleyl alcohol, methyl ether	Aliphatic	X		X	
Pentacosanoic acid, methyl ester	Aliphatic	X			
Pentadecane, 7-methyl-	Aliphatic				X
Pentanoic acid, 2,2,4-trimethyl-3-carboxyisopropyl, isobutyl ester	Aliphatic			X	
Pentatriacontane	Aliphatic	X		X	
Tetracontane	Aliphatic	X		X	
Tetracosanoic acid, methyl ester	Aliphatic	X		X	
Tetradecane	Aliphatic			X	
Tetradecane, 2,2-dimethyl-	Aliphatic			X	
Triacontanoic acid, methyl ester	Aliphatic				X
Phenol, 2,4-bis(1,1-dimethylethyl)-	Aromatic	X			X
Phthalic acid, butyl 4-octyl ester	Aromatic	X			
Hexadecanoic acid, 2-hydroxyethyl ester	Cutin derived	X	X		X
n-Hexadecanoic acid	Cutin derived			X	
Benzoic acid, 4-hydroxy-3-methoxy-, methyl ester	Lignin derived	X	X	X	X
13-Docosenamide, (Z)-	N-bearing	X			
2,2-Dimethyl-N-ethylpyrrolidine	N-bearing		X		
3-Cyclopentylpropionamide, N,N-dimethyl-	N-bearing		X		
4-Methoxybenzylamine, N,N-dibutyl-	N-bearing	X	X	X	
4-Morpholineethanamine	N-bearing				X
5,10-Diethoxy-2,3,7,8-tetrahydro-1H,6H-dipyrrolo[1,2-a:1',2'-d]pyrazine	N-bearing	X	X	X	X
9H-Purin-6-amine, N,N,9-trimethyl-	N-bearing	X	X	X	X
Caffeine	N-bearing	X	X	X	X
Decanamide-	N-bearing	X			
Hexadecanamide	N-bearing		X		X
Morpholine	N-bearing		X		
Morpholine, 4-(1-hydroxypropyl)-	N-bearing		X		
Morpholine, 4-acetyl-	N-bearing		X		
N,N-Dimethyldodecanamide	N-bearing	X	X	X	
N-Formylmorpholine	N-bearing	X			X
Octadecanamide	N-bearing	X		X	
Octanamide, N,N-dimethyl-	N-bearing				X
Piperazine-2,5-dione, 1,4-dimethyl-3,3'-bis-	N-bearing			X	

Methyl stearate	Suberin derived	X	X	X	X
Octadecane	Suberin derived	X			
Octadecanoic acid	Suberin derived	X		X	X
2,2,4-Trimethyl-1,3-pentanediol diisobutyrate	Unk.	X	X		
2,2-Dimethyloctadecane	Unk.				X
5,5-Diethylheptadecane	Unk.	X			
l-(+)-Ascorbic acid 2,6-dihexadecanoate	Unk.	X	X		
Cyclopropaneoctanoic acid, 2-[[2-[(2-ethylcyclopropyl)methyl]cyclopropyl]methyl]-, methyl ester	Unk.				X
Oxirane, [[(2-ethylhexyl)oxy]methyl]-	Unk.			X	
Pentanoic acid, 2,2,4-trimethyl-3-carboxyisopropyl, isobutyl ester	Unk.				X

Supplementary Table 6. Main products released from off line Thermochemolysis (TMAH-GC/MS), within the third distance (6 – 15 mm).

Name	Origin	+Pl/+N	-Pl/+N	+Pl/-N	-Pl/-N
10-Methylnonadecane	Aliphatic	X			X
1-Cyclopentyleicosane	Aliphatic	X			
1-Docosanol, methyl ether	Aliphatic	X	X	X	X
1-Heptacosanol	Aliphatic	X	X	X	X
1-Hexadecanol	Aliphatic	X			
2,2,4-Trimethyl-1,3-pentanediol diisobutyrate	Aliphatic	X	X		
2-Hexanol, 2,5-dimethyl-, (S)-	Aliphatic		X		
3-Heptanone, 2-methyl-	Aliphatic		X		
4-Octanone	Aliphatic	X			
7,10-Octadecadienoic acid, methyl ester	Aliphatic	X			
Docosane	Aliphatic			X	
Docosanoic acid, methyl ester	Aliphatic			X	
Eicosane	Aliphatic	X	X	X	X
Heptadecane	Aliphatic	X	X	X	X
Heptadecane, 3-methyl-	Aliphatic	X			
Heptadecane, 8-methyl-	Aliphatic	X		X	
Hexacosane	Aliphatic	X			
Hexadecane, 2,6,11,15-tetramethyl-	Aliphatic	X			
Methyl 18-methylnonadecanoate	Aliphatic	X	X	X	X
Nonane, 3-methyl-5-propyl-	Aliphatic			X	

Octacosanoic acid, methyl ester	Aliphatic			X	
Oleyl alcohol, methyl ether	Aliphatic	X			
Pentacosanoic acid, methyl ester	Aliphatic	X			X
Pentadecanal-	Aliphatic	X			
Pentanoic acid, 2,2,4-trimethyl-3-carboxyisopropyl, isobutyl ester	Aliphatic			X	
Pentanoic acid, 5-hydroxy-, 2,4-di-t-butylphenyl esters	Aliphatic	X			
Pentatriacontane	Aliphatic	X			
Tetracontane	Aliphatic	X		X	X
Tetracosanoic acid, methyl ester	Aliphatic	X	X	X	X
Tetradecane	Aliphatic				X
Tetrapentacontane	Aliphatic			X	X
Tetratriacontane	Aliphatic	X			
Triacontanoic acid, methyl ester	Aliphatic			X	
Tridecanol, 2-ethyl-2-methyl-	Aliphatic	X			
Undecane, 2,8-dimethyl-	Aliphatic	X			
cis-9-Hexadecenal	Aliphatic		X		
Heneicosanoic acid, methyl ester	Aliphatic		X		
Heptadecane, 2,6,10,15-tetramethyl-	Aliphatic		X		
Tetracosanoic acid	Aliphatic		X		
Tetradecane, 2,2-dimethyl-	Aliphatic		X		
Dodecane, 2,2,11,11-tetramethyl-	Aliphatic Compounds				X
Dotriacontane	Aliphatic Compounds				X
N,N-Dimethyldodecanamide	Aliphatic Compounds				X
Nonadecane, 9-methyl-	Aliphatic Compounds				X
n-Tetracosanol-1	Aliphatic Compounds				X
Phenol, 2,4-bis(1,1-dimethylethyl)-	Aromatic		X		
Hexacosanoic acid, methyl ester	Cutin derived		X	X	X
Hexadecanoic acid, 2-hydroxyethyl ester	Cutin derived			X	X
n-Hexadecanoic acid	Cutin derived	X		X	X
Benzoic acid, 4-hydroxy-3-methoxy-, methyl ester	Lignin Derived	X	X	X	X
2,4(1H,3H)-Pyrimidinedione, 1,3,5-trimethyl-	N-bearing				X
2-Pyrrolidinecarboxylic acid, 1,2-dimethyl-5-oxo-, methyl ester	N-bearing	X			

4-Methoxybenzylamine, N,N-dibutyl-	N-bearing	X		X	X
4-Morpholineethanamine	N-bearing			X	X
5,10-Diethoxy-2,3,7,8-tetrahydro-1H,6H-dipyrrolo[1,2-a:1',2'-d]pyrazine	N-bearing	X	X	X	X
9H-Purin-6-amine, N,N,9-trimethyl-	N-bearing	X		X	X
Caffeine	N-bearing		X	X	X
Morpholine, 4-acetyl-	N-bearing	X	X		
N-Formylmorpholine	N-bearing	X	X	X	
Octadecanamide	N-bearing	X		X	X
Octanamide, N,N-dimethyl-	N-bearing			X	
Piperazine-2,5-dione, 1,4-dimethyl-3,3'-bis-	N-bearing	X			
Acetaldehyde, ethylidenehydrazone	N-bearing		X		
Methyl stearate	Suberin derived			X	X
Octadecanoic acid	Suberin derived	X		X	X
Phthalic acid, 6-ethyl-3-octyl heptyl ester	Unknown		X		
Phthalic acid, butyl nonyl ester	Unknown	X			
5,5-Diethylheptadecane	Unknown			X	
Butane, 2,2-dimethyl-	Unknown		X		
Cyclopropane, 1-(1-methylethyl)-2-nonyl-	Unknown		X		
Ether, butyl isopentyl	Unknown		X		
Nonane, 3,7-dimethyl-	Unknown		X		
Butanoic acid, 3-methyl-, 2-methylbutyl ester	Unknown		X		